RADC-TR-81-196
Final Technical Report
July 1981

(12) LEVEL II

EVALUATION OF HALO DECONVOLUTION SCHEMES

Bolt Beranek & Newman, Inc.

Sponsored by
Defense Advanced Research Projects Agency (DoD)
ARPA Order No. 3655

The views and conclusions contained in this document are those of the authors and should not be interpreted as necessarily representing the official policies, either expressed or implied, of the Defense Advanced Research Projects Agency or the U. S. Government.

ROME AIR DEVELOPMENT CENTER
Air Force Systems Command
Griffiss Air Force Base, New York 13441

EVALUATION OF HALO DECONVOLUTION SCHEMES

This report has been reviewed by the RADC Public Affairs Office (PA) and is releasable to the National Technical Information Service (NTIS). At NTIS it will be releasable to the general public, including foreign nations.

RADC-TR-81-196 has been reviewed and is approved for publication.

APPROVED: Doris Hamill

DORIS HAMILL, Capt, USAF
Project Engineer

APPROVED: Frank J Rehm

FRANK J. REHM
Technical Director
Surveillance Division

FOR THE COMMANDER: John P. Huss

JOHN P. HUSS
Acting Chief, Plans Office

If your address has changed or if you wish to be removed from the RADC mailing list, or if the addressee is no longer employed by your organization, please notify RADC (OCSE) Griffiss AFB NY 13441. This will assist us in maintaining a current mailing list.

Do not return this copy. Retain or destroy.

EVALUATION OF HALO DECONVOLUTION SCHEMES

Dr. Richard Barakat

Contractor:	Bolt Beranek and Newman Inc.
Contract Number:	F30602-79-C-0018
Effective Date of Contract:	29 Nov 78
Contract Expiration Date:	15 Nov 80
Short Title of Work:	Wavefront Deconvolution Studies
Program Code Number:	OE20
Period of Work Covered:	Nov 78 - Nov 80
Principal Investigator:	Dr. Richard Barakat
Phone:	(617) 491-1850
Project Engineer:	Doris Hamill, Capt., USAF
Phone:	(315) 330-3148

This research was supported by the Defense Advanced Research Projects Agency of the Department of Defense and was monitored by Capt Doris Hamill (RADC/OCSE), Griffiss AFB NY 13441 under Contract F30602-79-C-0018.

UNCLASSIFIED

SECURITY CLASSIFICATION OF THIS PAGE (When Data Entered)

REPORT DOCUMENTATION PAGE

READ INSTRUCTIONS BEFORE COMPLETING FORM

1. REPORT NUMBER: RADC-TR-81-196

2. GOVT ACCESSION NO.: AD-A105 125

3. RECIPIENT'S CATALOG NUMBER:

4. TITLE (and Subtitle): EVALUATION OF HALO DECONVOLUTION SCHEMES

5. TYPE OF REPORT & PERIOD COVERED: Final Technical Report, Nov 78 — Nov 80

6. PERFORMING ORG. REPORT NUMBER: N/A

7. AUTHOR(s): Dr. Richard Barakat

8. CONTRACT OR GRANT NUMBER(s): F30602-79-C-0018, ARPA Order 3655

9. PERFORMING ORGANIZATION NAME AND ADDRESS: Bolt Beranek and Newman, Inc., 10 Moulton Street, Cambridge MA 02238

10. PROGRAM ELEMENT, PROJECT, TASK AREA & WORK UNIT NUMBERS: 62301E, C2230108, 01

11. CONTROLLING OFFICE NAME AND ADDRESS: Defense Advanced Research Projects Agency, 1400 Wilson Blvd., Arlington VA 22209

12. REPORT DATE: July 1981

13. NUMBER OF PAGES: 136

14. MONITORING AGENCY NAME & ADDRESS (if different from Controlling Office): Rome Air Development Center (OCSE), Griffiss AFB NY 13441

15. SECURITY CLASS. (of this report): UNCLASSIFIED

15a. DECLASSIFICATION/DOWNGRADING SCHEDULE: N/A

16. DISTRIBUTION STATEMENT (of this Report)

Approved for public release; distribution unlimited.

17. DISTRIBUTION STATEMENT (of the abstract entered in Block 20, if different from Report)

Same

18. SUPPLEMENTARY NOTES

RADC Project Engineer: Doris Hamill, Capt, USAF (OCSE)

19. KEY WORDS (Continue on reverse side if necessary and identify by block number)

Wavefront Deconvolution
Zernike Polynomials
Singular Value Decomposition
Wavefront Aberrations

20. ABSTRACT (Continue on reverse side if necessary and identify by block number)

The final report chronicles various aspects of the research conducted by the principal investigator on the wavefront deconvolution problem. Only work carried out since the interim report RADC-TR-80-154, May 1980, was released is discussed because the material in the interim report is complete in itself. The work discussed here naturally forms four major interrelated, but separate research items, and each topic is the subject of a separate section of the final report. In addition, there is an appendix

DD FORM 1 JAN 73 1473 EDITION OF 1 NOV 65 IS OBSOLETE

UNCLASSIFIED

SECURITY CLASSIFICATION OF THIS PAGE (When Data Entered)

060100

cont.

devoted to a minor item which evolved during the course of the investigation but is not directly related to the major items.

GENERAL INTRODUCTION

The final report chronicles various aspects of the research conducted by the principal investigator on the wavefront deconvolution problem. Only work carried out since the interim report RADC-TR-80-154, May 1980 was released, is discussed because the material in the interim report is complete in itself. The work discussed here naturally forms four major interrelated, but separate research items, and each topic is the subject of a separate section of the final report. In addition, there is an appendix devoted to a minor item which evolved during the course of the investigation but is not directly related to the major items.

The four major sections and appendix are entitled:

Section 1: Imperfectly known Fourier transform pairs with application to deconvolution.

Section 2: Interferogram reduction for aberrated annular apertures via Zernike-Barakat functions using L_2 and L_1 norm algorithms.

Section 3: Upper and lower bounds on radially symmetric optical transfer functions.

Section 4: Moment estimator approach to the retrieval problem in coherence theory.

Appendix: The Shannon number of an incoherent diffraction image.

Finally, there is a section which summarizes and integrates the technical work performed during the contract since its inception.

SECTION 1

IMPERFECTLY KNOWN FOURIER TRANSFORM PAIRS WITH APPLICATIONS TO DECONVOLUTION

ABSTRACT

An algorithm for extrapolation of partially known, band-limited functions based upon singular value decomposition of finite Fourier transforms is outlined. The decomposition is used to make rational choices for a discretization of the problem and to make prior estimates of errors. The algorithm provides a systematic approach to the ill posed problem of extrapolation of noisy data. In this, it is an improvement over previously proposed iterative algorithms such as the G-S algorithm. Some numerical results are presented for two situations (with obvious optical diffraction interpretations) to illustrate the main features of the algorithm.

1. INTRODUCTION

The retrieval of wavefront aberrations from the measured point spread function of an optical system has been the subject of several recent papers since the important work of Gonsalves [1]. Gonsalves employed two different retrieval methods: parameter search technique and the Gerschberg-Saxon (GS) iterative technique. Both methods are quite sensitive to noise in the measurements. An alternative method was developed by Barakat and Newsam [2] in research sponsored by RADC, which attacked the problem as a nonlinear least squares estimation problem using a filtered version of singular value decomposition. The BN approach rests upon two provisos: (1) the aberrated wavefront itself is the primary objective of the inversion and not an assumed functional form of it as Gonsalves [1], and Southwell [3]; (2) the nonlinear inversion method is tailored to be robust with respect to noise in the measured point spread function. The representative calculations discussed and displayed in [2] show ample testimony to the usefulness of this mathematically elaborate approach. The extension of the BN approach to time adaptive imaging is presently under investigation.

Given these preliminary remarks, we are convinced that the GS algorithm or some alternative has potential usefulness in the active optics deconvolution scheme. Private discussions with several investigators who have employed the GS algorithm (some in the optics area and others in the electron microscopy area) have indicated a sort of hit-or-miss attitude with respect to the behavior of the algorithm in various situations. Sometimes the algorithm works and sometimes it fails when the data are noisy. With possible exception of Youla's recent study [4], there are really no serious attempts to understand the stability of the GS algorithm with respect to noise in the measurements. The work of Papoulis [5], although extremely interesting simply does not address these types of questions which are so vital if GS type algorithms are to be used in deconvolution schemes of adaptive optics.

We feel that an alternate algorithm can be developed which, as in the BN algorithm, can be made robust with respect to noisy data by starting *ab initio*. The purpose of this chapter is to outline *some* aspects of the new algorithm and to present numerical data for one typical situation. Because the current contract has been terminated extensions of the analysis to more complicated situations is held in abeyance.

2. MODEL PROBLEM AND ASSOCIATED THEORY

The model problem for extension of finite Fourier transforms is:

Given a function $\hat{g}(v)$ measured on $v \varepsilon A \equiv [a_1, a_2]$ that is known to be the Fourier transform of a function $G(\omega)$ which has support contained in $B \equiv [b_1, b_2]$, extend $\hat{g}(v)$ to a function $g(v)$ defined on the entire real axis.

Because B is a bounded set, $\hat{g}(v)$ is analytic by the Paley-Wiener theorem [6]; consequently a unique extension exists. However, the problem is therefore one of analytic continuation which is known to be highly sensitive to measurement error in $\hat{g}(v)$, see [7,8]. This is a strong argument for an algorithm with a clear direct treatment of noise included as part of the formulation.

The following notation is introduced.

Definition 1. Let $G(\omega) \varepsilon L^2$, the Fourier transform $g(v)$ of $G(\omega)$ is defined as

$$g(v) \equiv \int_{-\infty}^{\infty} e^{2\pi i v \omega} G(\omega) d\omega \qquad (2.1)$$

and denoted by

$$g = FG \tag{2.2}$$

The inverse transform is denoted by

$$G = F^{-1}g \tag{2.3}$$

Definition 2. Let S be a subset of the real line. The projection operator on L^2 associated with S is denoted by P_S and defined by

$$\begin{aligned}(P_S f)(v) &= f(v) \qquad v\varepsilon S \\ &= 0 \qquad\quad v\not\in S\end{aligned} \tag{2.4}$$

In this notation, the model problem is: Given a measurement $\hat{g}$ find g and G such that

$$\hat{g} = P_B F P_A G \quad , \quad g = F P_A G \tag{2.5}$$

The problem can be symmetrized using simple translations and scaling to read: Given a measurement $\hat{g}$ find g, G such that

$$\hat{g} = P_c F P_c G \quad , \quad g = F P_c G \tag{2.6}$$

where

$$C = [-c,c], \; c \equiv \frac{1}{2}\left[(a_2-a_1)(b_2-b_1)\right]^{\frac{1}{2}} \tag{2.7}$$

In order to make quantitative judgments on noise and ill conditioning in Eq. 2.6, we shall use the concepts of singular value decomposition. We assume the reader is familiar with this method of analysis applied to either infinite dimensional compact linear operators or to finite matrices; a discussion of the first case can be found in Baker [9], of the second in Stewart [10].

In a series of papers, Landau *et al.* [11,12], the structure of $P_c F P_c$ was fully exposed. The key results are repeated here for convenience:

1) $P_c F P_c$ is a normal compact operator, and

$$||P_c F P_c||_2 \leq 1 \tag{2.8}$$

2) The eigenfunctions of $P_c F P_c$ can be taken as real. They are then the prolate spheriodal wavefunctions here denoted by $\phi_n(v,c)$, making explicit the dependence on c.

3) The eigenvalues $\lambda_n(c)$ satisfy

$$\lambda_n(c) = e^{i\pi n/2}|\lambda_n| \tag{2.9}$$

$$|\lambda_n| > |\lambda_{n+1}|$$

4) The singular values are denoted by $\sigma_n(c)$ with

$$\sigma_n(c) \equiv |\lambda_n(c)| \tag{2.10}$$

They behave as follows

a. For a fixed c and increasing n

$$\sigma_n(c) \sim (c^2/n)^{2n} \tag{2.11}$$

b. For a fixed n, there exist constants α_n, β_n such that

$$\sigma_n(c) \geq 1-\alpha_n e^{-\beta_n c^2} \quad , \forall c \tag{2.12}$$

Since $P_c F P_c$ is compact, it has a singular value decomposition U, Σ, V where U and V are complete sets of orthonormal functions and Σ is the decreasing sequence of nonnegative numbers defined in Eq. 2.10. Since $P_c F P_c$ is normal,

$$\begin{aligned} U &= \left\{ u_n \phi_n(v,c) \right\}_{n=0}^{\infty} \\ V &= \left\{ v_n \phi_n(v,c) \right\}_{n=0}^{\infty} \end{aligned} \tag{2.13}$$

where u_n and v_n are constants such that $|u_n|=|v_n|=1$. With this machinery, the solution to the problem, see Eq. 2.6, can theoretically be determined by expanding $\hat{g}$ and G as

$$\hat{g} = \sum_{n=0}^{\infty} a_n v_n \phi_n(v,c) \tag{2.14}$$

$$G = \sum_{n=0}^{\infty} b_n u_n \phi_n(v,c) \tag{2.15}$$

determining the coefficients directly from the known $\hat{g}$ and the b_n from the relations

$$g = P_c F P_c G \Longleftrightarrow P_c F P_c (b_n u_n \sigma_n) \tag{2.16}$$

which in turn imply

$$b_n = \frac{a_n}{b_n} \cdot \frac{v_n}{u_n} \tag{2.17}$$

In this representation of the solution, the degree of ill conditioning and the effect of noise in Eq. 2.16 are deduced from the behavior of σ_n. Since $P_c F P_c$ is compact $\sigma_n \to 0$; therefore a small error in the coefficient a_n of a high frequency (large n) component $a_n v_n \phi_n(v,c)$ of $\hat{g}(v)$ will induce a large error in the coefficient b_n, as given by Eq. 2.17, of the corresponding component of G. If the random error in measurement is assumed to appear over all components of $\hat{g}$, then the calculated high frequency components of G are not to be trusted. But as the decomposition allows a direct observation of the effects of noise, so also does it allow direct action to reduce these effects; a filter $f(\sigma,\varepsilon)$

dependent on the noise level ε in $\hat{g}$ is introduced so that G is estimated by G'

$$G'(\omega) = \sum_{n=0}^{\infty} a_n \left(\frac{v_n}{u_n}\right) f(\sigma_n)\phi_n(\omega,c) \tag{2.18}$$

where

$$\begin{aligned} f(\sigma_n) &\to (\sigma_n)^{-1} \quad \text{as } \sigma_n \to 1 \\ &\to 0 \qquad\quad \text{as } \sigma_n \to 0 \end{aligned} \tag{2.19}$$

Choice of filters is an art, so we shall only note that if $f(\sigma_n,\varepsilon) = 0$ for $\sigma_n \leq \sigma_N$ then the system, Eq. 2.18, is said to have N-1 essential degrees of freedom [21], these can be used as an estimate of ill conditioning. A more general estimate is the rate of decay of σ_n, the larger the rate of decay the more ill conditioned the system.

In view of this analysis, the major conclusions to be drawn are:

1. $P_c F P_c$ is badly ill conditioned since $\sigma_n(c)$ exhibit exponential decay.

2. For a given c and noise level ε, the number $n(\varepsilon,c)$ of singular values significantly greater than ε can be bounded above by Eq. 2.12.

3. For a given c,ε the singular values are approximately distributed as a step function, i.e.,

$$\begin{aligned} n < n(\varepsilon,c) &\Rightarrow \quad \sigma_n(c) \sim 1 \\ n > n(\varepsilon,c) &\Rightarrow \quad \sigma_n(c) \sim 0 \end{aligned} \tag{2.20}$$

The algorithm proposed is based upon the following procedure. For a given c and ε, n(ε,c) is calculated. If it is sufficiently small, then accurate *numerical* approximations to σ_n, ϕ_n (v,c) are calculated for $n < n(\varepsilon,c)$ and G is estimated by Eq. 2.18 using a filter of the form

$$\begin{aligned} f(\sigma,\varepsilon) &= \frac{1}{\sigma} \qquad \sigma > \varepsilon \\ &= 0 \qquad \sigma < \varepsilon \end{aligned} \tag{2.21}$$

The algorithm is optimal in that it focuses on accurately calculating components of $\hat{g}$ that are significant in estimating G and ignoring components that are useless for estimation.

We conclude this section with a discussion of the theory of the Gerschberg-Saxton algorithm from our viewpoint and notation [13]. The algorithm estimates G_{n+1}, g_{n+1} from G_n, g_n by the following update

$$g_{n+1} = P_c F P_c G_n + \hat{g}, \; g_0 = 0 \tag{2.22}$$

$$G_{n+1} = P_c F^{-1} g_{n+1} \quad , G_0 = 0 \tag{2.23}$$

where $\bar{C}$ is the complement of C.

Concatenating these two equations yields

$$G_{n+1} = P_c F^{-1}(P_{\bar{c}} F P_c G_n + \hat{g}), \; G_0 = 0 \tag{2.24}$$

which in turn implies

$$G_{n+1} = (I - P_c F^{-1} P_c F P_c) G_n + P_c F^{-1} P_c \hat{g}, \tag{2.25}$$

noting that

$$P_c G_n = G_n \quad , P_c \hat{g} = \hat{g} \tag{2.26}$$

$$P_c + P_{\bar{c}} = I \quad \text{(identity operator)} \tag{2.27}$$

Equation 2.25 has a computational advantage over the previous equations in that it only requires evaluation of functions on the bounded set C instead of the infinite domain $\bar{C}$.

Equation 2.25 is recognizable as the simplest form of iterative solution of the normal equations associated with Eq. 2.6, that is

$$P_c F^{-1} P_c \hat{g} = P_c F^{-1} P_c F P_c G \tag{2.28}$$

The normal equations are usually not formed for ill conditioned systems since they have even poorer conditioning because if $P_c F P_c$ has singular value σ_n, then the singular value associated with $P_c F^{-1} P_c F P_c$ is σ_n^2. However since the σ_n display the step-like behavior noted above, for almost all significantly non-zero singular values $\sigma_n \sim \sigma_n^2 \sim 1$, so little is lost in considering Eq. 2.6.

In the presence of noise, Eq. 2.25 is usually modified so that it either stops when

$$||G_n - G_{n+1}|| \leq \delta \tag{2.29}$$

or, a $\lambda > 0$ chosen and the revised scheme

$$G_{n+1} = (1-\lambda)G_n - P_c F^{-1} P_c F P_c G_n + P_c F^{-1} P_c \hat{g} \tag{2.30}$$

used, where δ and λ depend upon the noise level ε. The second algorithm, if iterated to completion, corresponds to a choice of

$$f(\sigma) = \frac{1}{\sigma+\lambda} \tag{2.31}$$

in Eq. 2.21. However, this is impossible in practice, and since there is no "good" theory linking termination after N steps with

noise levels ε, the clear insights used to modify singular value decomposition solutions in the presence of noise cannot be applied to these alternative schemes. One important consequence of this lack of theory is that it is not possible to tell *a priori* how much computation is needed to reach a desired solution, since neither the number of iterations or the accuracy at each such iteration can be determined as a function of known noise levels.

There is a large literature on alternative techniques for Eqs. 2.6 and 2.28 which is summarized in Patterson [14]. The most attractive is the conjugate gradient method

$$r_n = P_c F^{-1} P_c \hat{g} - P_c F^{-1} P_c F G_n \quad , \tag{2.32}$$

where

$$G_{n+1} = G_n + \alpha_n p_n$$

$$p_{n+1} = r_{n+1} + \beta_n p_n \quad , \tag{2.33}$$

and

$$\alpha_n \equiv \frac{||r_n||^2}{||P_c F P_c p_n||^2} \quad , \quad \beta_n \equiv \frac{||r_{n+1}||^2}{||r_n||^2} \quad . \tag{2.34}$$

The initial conditions are:

$$r_0 = P_c F^{-1} P_c \hat{g} \quad , \quad G_0 = 0, \; p_0 = r_0 \quad . \tag{2.35}$$

We mention it here, as it is both an iterative algorithm and a Galerkin approximation and so can be examined using the analysis of the next section.

3. DISCRETE PROBLEM AND ASSOCIATED THEORY

This section is concerned with the formation of finite dimensional approximations to Eq. 2.6, their solution, and the relative merits of different approximations to Eq. 2.6. Since the natural error metric for Eq. 2.6 is $||\cdot||_2$, all discretizations considered are derived using Galerkin's method. The procedure is to choose two sets of linearly independent functions

$$\{\psi_k\}_{k=1}^{K} \quad , \quad \{\theta_\ell\}_{\ell=1}^{L} \; ; \; ||\psi_k|| = ||\theta_\ell|| = 1 \tag{3.1}$$

and define the following quantities:

Definition 3. Let S_K denote the subspace spanned by $\{\psi_k\}_{k=1}^{K}$, S_L the subspace spanned by $\{\theta_\ell\}_{\ell=1}^{L}$; let P_K denote the projection operator from L_2 onto S_K, Q_L the projection operator from L_2 on S_L.

Approximations

$$\hat{g}_K \in S_K \rightarrow \hat{g}, G_L \in S_L \rightarrow G \tag{3.2}$$

are now generated by requiring that

$$\hat{g}_K = P_K \hat{g} \quad , \; P_K \hat{g} = P_K P_c \, F P_c G_L \tag{3.3}$$

These equations can be cast into matrix form

$$\tilde{\tilde{B}}\tilde{b} = \tilde{c} \quad , \quad \tilde{c} = \tilde{\tilde{D}}\tilde{a} \quad , \tag{3.4}$$

by defining

$$\hat{g}_K = \sum_{k=1}^{K} b_k \psi_k \quad , \quad G_L = \sum_{\ell=1}^{L} a_\ell \theta_\ell$$

$$c_k = (\psi_k, \hat{g}) \quad , \quad B_{ij} = (\psi_i, \psi_j)$$

$$A_{ij} = (\theta_i, \theta_j) \quad , \quad D_{k\ell} = (\psi_k, P_c F P_c \theta_\ell) \quad , \tag{3.5}$$

where $(\cdot,\cdot)$ denotes the inner product on L^2.

Each such Galerkin approximation implicitly defines an associated finite rank operator R_{KL} such that

$$R_{KL} = P_K P_c F P_c Q_L \tag{3.6}$$

$$P_K \hat{g} = R_{KL} G_L \quad . \tag{3.7}$$

R_{KL} depends only upon the subspaces S_K, S_L and not on the particular choice of bases $\{\psi_k\}$, $\{\theta_\ell\}$ as do the matrices $\tilde{A}, \tilde{B}, \tilde{D}$. In the formulation, there is considerable freedom of choice for these subspaces and bases; it is therefore appropriate to adopt criteria by which a particular choice can be judged. Five such criteria will be used, but before judgment is made it is necessary to distinguish between the presence and absence of noise.

A choice is first made in the absence of noise, then in light of a known noise level. The criteria are:

1. Accuracy of approximation: It seems reasonable to require that a particular approximation be part of a sequence of approximations that satisfy

$$\lim_{K,L\to\infty} ||R_{KL}-P_c F P_c|| \to 0 \quad . \tag{3.8}$$

If Eq. 2.6 possesses a solution G, then

$$\lim_{K,L\to\infty} ||G-G_L|| \to 0 \quad . \tag{3.9}$$

These conditions may be difficult, if not impossible, to prove for the general choice; however, the following proposition (stated without proof) shows at least one such basis exists:

Proposition 1: If K = L = N and ψ_k, θ_ℓ are chosen so that $\psi_k(v) = \theta_k(v) = \phi_k(v)$ then the Galerkin approximation generated by Eq. 3.3 satisfies Eqs. 3.8 and 3.9. Furthermore,

$$||R_{NN}-P_c F P_c|| \leq ||R_{K'L'}-P_c F P_c|| \tag{3.10}$$

for any other choice of $S_{K'}$, $S_{L'}$ with

$$\dim(S_{K'}) = K' \leq N \quad ; \quad \dim(S_{L'}) = L' \leq N \tag{3.11}$$

2. Conditioning of $\tilde{A},\tilde{B},\tilde{D}$: The previous criterion indicate whether or not S_K, S_L are good choices as approximating subspaces, but says nothing about a particular choice of bases within those subspaces. It is possible to choose ψ_k, θ_ℓ so that $\tilde{D}$ is well conditioned; but this is an illusory gain since the matrices $\tilde{B}$ and/or $\tilde{A}$ will then be ill-conditioned. Therefore, calculations of $\hat{g}_K(v)$, $G_L(v)$ made using the representations given in Eq. 3.5 will be inaccurate. There is not a good figure for comparison of ill-conditioning induced by different bases, but some indication of the dependence follows from propositions 2 and 3 (stated without proof):

Proposition 2: Let S_K, S_L be fixed subspaces; $\{\psi_k\}_{k=1}^{K}$, $\{\theta_\ell\}_{\ell=1}^{L}$ be orthonormal bases for S_K, S_L. Also let $\{\psi'_k\}_{k=1}^{K}$, $\{\theta'_\ell\}_{\ell=1}^{L}$ be be any other bases for S_K, S_L. If $\tilde{A}$, $\tilde{A}'$, $\tilde{B}$, $\tilde{B}'$, $\tilde{D}$, $\tilde{D}'$ are the corresponding matrices defined by Eq. 3.5, then

$$\det(\tilde{B}'\tilde{D}'\tilde{A}') \leq \det(\tilde{B}\tilde{D}\tilde{A}) = \det(\tilde{D}) \quad . \tag{3.12}$$

Proposition 3: Let $\psi_k = \theta_k = \phi_k$, $K = L = N$ and $\tilde{D}$ be the matrix formed in Eq. 3.5. Let $\{\psi'_k\}_{k=1}^{K'}$ $\{\theta'_\ell\}_{\ell=1}^{L'}$ be any other choice of orthonormal basis such that $K', L' \geq N$, then

$$\det(\tilde{D}) \geq \det(\tilde{D}') \quad . \tag{3.13}$$

3. Desirable special results: Particular choices of ψ_k, θ_ℓ give special results that are often desirable. If both bases are orthogonal, then it is easily shown that the singular values of $\tilde{D}$ are the same as those of R_{KL} which in turn approximate the first few singular values of $P_c F P_c$. If K = L and ψ_k, θ_k are chosen so that

$$\psi_k = P_c F P_c \theta_k \tag{3.14}$$

then the Galerkin approximation is also a least squares solution, i.e.,

$$||\hat{g} - P_c F P_c G_L|| \leq ||\hat{g} - P_c F P_c H|| \quad , \forall H \epsilon S_L \ . \tag{3.15}$$

Again if the Galerkin approximation is generated using the eigenvectors as the bases then both these results hold.

4. Ease of computation: In spite of the advantages of using eigenfunctions to form an approximation as outlined above. we do not consider their use in actual computation because there is no known simple algorithm for their numerical evaluation. Since numerical evaluation of Fourier transforms and orthonormalization are computationally expensive, it is convenient to choose $\{\theta_\ell\}_{\ell=1}^{L}$ to be an orthonormal set of simple functions whose Fourier transforms can be evaluated analytically. However, the finite Fourier transform of a simple function is itself often

not simple, so the inner products $(\psi_k, P_c F P_c \theta_\ell)$ must ultimately be done numerically.

5. Ease of extrapolation: Because it is desired to extrapolate $\hat{g}(v)$ to a function $g(v)$ on the entire real line, a choice of simple θ_ℓ will allow analytic computation of the approximation

$$g_L = F P_c G_L \tag{3.16}$$

to g; numerical computation could again be expensive.

For the noiseless case, the issues raised by the above criteria lead to the following sequence of bases and Galerkin approximations to the solution of Eq. 2.6. First, choose a $\det\{\rho_k\}_{k=1}^{\infty}$ that is a complete orthonormal basis of simple functions for $L^2(c)$ with the property that each eigenfunction can be expressed as a rapidly convergent series in ρ_k. If possible, also require that $P_c F P_c \rho_k$ is close to $c_k \rho_k$, where c_k is a constant. Second, for a given N choose a K(N) such that the first N eigenfunctions are well approximated by $\{\rho_k\}_{k=1}^{K(N)}$. Choose $\psi_k = \theta_k = \rho_k$ and form the $\tilde{c}$ and $\tilde{D}$ of Eq. 3.5. Find the singular value decomposition of $\tilde{D} = \tilde{U}\tilde{\Sigma}\tilde{V}^+$. It can be shown that if the approximation is sufficiently accurate, the largest N singular values and associated singular functions are the approximations to the first N σ_n, ϕ_n. Therefore, the

remaining singular values Σ_{kk} of $\tilde{D}$ are set equal to zero and the system $\tilde{c} = \tilde{D}\tilde{a}$ solved in a least squares sense,

$$\tilde{a} = \tilde{V}\tilde{\Sigma}^{\oplus}\tilde{U}^{+}\tilde{c} \quad , \tag{3.17}$$

where

$$\Sigma^{\oplus}_{kk} = \Sigma^{-1}_{kk} \text{ if } \Sigma_{kk} \neq 0$$

$$= 0 \quad \text{if } \Sigma_{kk} = 0 \ . \tag{3.18}$$

If the above conditions on $\{\rho_k\}$ are satisfied, one can show that the sequence of approximate solutions G_N so generated, converges to the true solution G if it exists.

In the case of a known noise level, the two-fold sequence listed in the first part of the previous paragraph is combined with the approach outlined in Sec. 2. Instead of generating a convergent sequence of approximations, a single approximation is found that is as accurate as possible in the presence of the given noise level. The number $N = n(\varepsilon,c)$ of singular values significantly greater than ε is calculated and K(N) is chosen so that the first N σ_n, ϕ_n are approximated to within some tolerance $\delta(\varepsilon)$ by $\{\rho_k\}$. $\tilde{D}$ is formed and decomposed as in the noise-free case; however, $\tilde{\Sigma}^{\oplus}$ is redefined as

$$\Sigma^{\oplus}_{kk} = \Sigma^{-1}_{kk} \quad \text{if } \Sigma_{kk} > \varepsilon$$

$$= 0 \quad \text{if } \Sigma_{kk} < \varepsilon \tag{3.19}$$

then the approximation

$$G_N = \sum_{k=1}^{K(N)} a_k \rho_k \tag{3.20}$$

is formed and $g_N = FG_N$ is evaluated.

The construction of an algorithm for the inversion of Eq. 2.6 in the presence of noise is now complete. The salient features are: use of the singular value decomposition of $P_c F P_c$, prior estimation of the number of degrees of freedom $n(\varepsilon,c)$ present at a given noise level, and construction of a Galerkin approximation from a predetermined number of functions that are computationally simple but also approximate the first $n(\varepsilon,c)$ eigenfunctions.

We conclude this section by noting that the conjugate gradient method discussed at the very end of Sec. 2 is also a Galerkin approximation, where $\psi_k = \theta_k = r_k$, for the solution of the normal equations, see Eq. 2.28. Although it has many of the features highlighted by our five criteria (e.g., it produces a sequence of approximations convergent to the solution, (if one exists), it does not allow the filtering of noise, an

estimate such as $n(\varepsilon,c)$ or $K(N)$ of the number of iterations needed, nor is it easily computed. In fact, in most iterative schemes a basis is implicitly used to represent the iterates; it would seem best then to directly form a Galerkin approximation using this basis.

4. ILLUSTRATIVE NUMERICAL CALCULATIONS

To illustrate the analysis of the previous sections, a particular basis set was chosen and its Galerkin approximation studied from two viewpoints: (1) analysis of the matrix $\tilde{D}$ of Eq. 3.5 and (2) solution of Eq. 2.6 using Eq. 3.16 in the presence of noise.

The basis chosen is the piecewise constant functions over [-c,c]. Since a complex-valued singular value decomposition code for matrices is not available, $\hat{g}$, G and g in Sec. 2 are taken to be real even functions. Item (1) above is not affected because the real matrix $\tilde{D}^{+}\tilde{D}$ could be formed and decomposed to recover the singular values. Although the singular values and singular vectors of $P_c F P_c$ split into even and odd subsets, the subsets display the same distribution so this restriction does not significantly change the inversion problem. The basic functions we employed are

$$\rho_k(\omega) = \left(\frac{N}{2c}\right)^{\frac{1}{2}} \quad , \quad \omega \varepsilon \left[\frac{2c(k-1)-cN}{N} \; , \; \frac{2ck-cN}{N}\right]$$
$$= 0 \quad , \quad \text{elsewhere} \quad . \tag{4.1}$$

The Galerkin approximation was formed as discussed in Sec. 3 by choosing K = L = N and $\psi_k = \theta_k = \rho_k$. The functions $P_c F P_c \rho_n$ were evaluated analytically. Consequently the vector $c_j = (\hat{g}, \rho_j)$ was produced, where 7 point Gauss quadrature was

used to integrate the inner products. From Secs. 2 and 3, the quantities of interest are the number of significantly nonzero singular values of $P_c F P_c$ for a fixed c. In addition, we wish to know how well they are approximated by the singular values of $\tilde{D}_N$ for a particular N.

The singular values of $\tilde{D}_N$ were numerically evaluated on a computer for various N and c values. Table 1 is a summary of the results. Recall that $n(\varepsilon,c)$ indicates the number of singular values of $P_c F P_c$ greater than ε, $N(\varepsilon,c)$ indicates the number of basis functions needed to insure that the singular values of $\tilde{D}_N$ are within an accuracy ε of those of $P_c F P_c$. Because it is impractical to consider every value of N, the table gives an interval containing $N(\varepsilon,c)$ rather than the exact result. The table indicates that the piecewise constant functions are by no means an optimal basis in that $N(\varepsilon,c)$ is not close to $n(\varepsilon,c)$. Nevertheless, it is adequate for large and small c. The piecewise constant functions, however, are a very good choice from a computational viewpoint. Furthermore, as we will shortly see, it appears that it is not necessary for the basis functions to be good approximations to the singular values in order to perform accurate inversions.

Two functions (with obvious optical interpretations) were chosen for numerical experimentation. They are:

$$g(v) = \frac{\sin 2\pi v}{\pi v} \tag{4.2a}$$

$$= 2\left(\frac{\sin \pi v}{\pi v}\right)^2 \quad . \tag{4.3a}$$

The corresponding Fourier transforms are

$$G(\omega) = 1 \quad , \quad |\omega| \leq 1$$

$$= 0 \quad , \quad |\omega| > 1 \tag{4.2b}$$

and

$$G(\omega) = 2(1-|\omega|) \quad , \quad |\omega| \leq 1$$

$$= 0 \qquad . \quad |\omega| > 1 \quad . \tag{4.3b}$$

In order to make the numerical results specific, we gated the g(v) functions to the finite interval $|v| \leq 1$ (i.e., c = 1 in Eq. 2.7).

Approximations to the G's were calculated using the Galerkin approximation generated by $\{\rho_k\}$ and Eq. 3.5. The filter of Eq. 2.21 was used with the cutoff taken to be the greater of the noise level δ(specified below) and the accuracy of the Galerkin approximation (taken to be $\sim 10^{-2}$ for these problems). Approximations to the true extrapolations g(v) in the range $|v| \leq 4$, were found from the exact Fourier transforms of the calculated G's, i.e.,

$$g_N = FG_N = \sum_{n=1}^{N} a_n F\rho_n \quad . \tag{4.4}$$

To simulate the presence of noise in the measurements of $\hat{g}(v)$, whenever a value of $\hat{g}(v)$ was required in the numerical integrations needed to calculate the vector $c_j = (\hat{g},\rho_j)$, a random perturbation was added. That is

$$\hat{g}_\delta(v) = \hat{g}(v) + \delta\mu \max_{v\in c} |\hat{g}(v)| \tag{4.5}$$

was used instead of g(v). The constant δ denotes the noise level, μ is a random variable uniformly distributed over [-1,1]. The effect of noise on the inversions and extrapolations was studied by comparing with the noiseless inversion/extrapolation as the standard. In all cases to be discussed, the noise level was 3%, $\delta = 0.03$.

Figure 1 shows four sample realizations of $G(\omega)$, corresponding to Eq. 4.2b, as calculated from the noisy $\hat{g}(v)$ using a basis of 40 piecewise constant functions. The $G(\omega)$ calculated in the absence of noise coincided with the true $G(\omega)$ to within less than 0.05%. Four reconstructions of $G(\omega)$ in the presence of 1% noise are listed in Table 2, and have about a 5% maximum deviation from the true value. The extrapolations of g(v) for two of these sample realizations in the presence of 3% noise are displayed in Figs. 2 and 3 (see open circles), with the exact g(v) shown as the solid line.

Figures 4 and 5 show the behavior of $G(\omega)$, Eq. 4.3b, as calculated from four sample realizations of $\hat{g}(v)$; this time with N = 80. As before, the noiseless calculations coincide with the true $G(\omega)$ to well within graphical accuracy. However, the extrapolation is not as well behaved, as witness Fig. 6. This is undoubtedly due to the fact that the true $G(\omega)$ has a discontinuity in slope at $\omega = 0$. Failure to reproduce the correct slope at the origin propagates an error throughout the remainder of the algorithm.

The extrapolations of the corresponding $g(v)$ for three of these sample realizations (in the presence of 3% noise) are show in Figs. 7 through 9 (see open circles) with the exact $g(v)$ shown as the solid line. We feel that the relatively poor extrapolations of $g(v)$ in this case are due to most of the error in $G(\omega)$ appearing at low frequencies which are then transformed into errors at the tail of $g(v)$.

We believe that a choice of basic functions that have the same degree of smoothness as the unknown $G(\omega)$ will tend to alleviate this problem. Work in continuing along these lines.

TABLE 1. DISTRIBUTION OF SINGULAR VALUES OF $P_C \mathcal{P} P_C$ AND REQUIRED BASIS SIZE FOR DESIRED ACCURACY.

c	$n(10^{-2},c)$	$N(10^{-2},c)$	$n(10^{-3},c)$	$N(10^{-3},c)$
.5	4	<10	5	10-20
1.0	8	30-40	9	60-80
1.5	13	60-80	15	>80
2.0	21	>80	23	>80

TABLE 2. FOUR SAMPLE REALIZATIONS OF RECONSTRUCTIONS WITH 1% NOISE.

ω	$G(\omega)$	$G(\omega)$	$G(\omega)$	$G(\omega)$
-1.0000	.983	.973	1.099	.907
- .9474	1.009	1.010	1.043	1.005
- .8947	1.013	1.021	.995	1.046
- .8421	1.004	1.017	.962	1.050
- .7895	.991	1.007	.944	1.035
- .7368	.980	.997	.942	1.013
- .6842	.974	.990	.952	.993
- .6316	.975	.989	.971	.980
- .5789	.980	.993	.995	.976
- .5263	.988	1.000	1.017	.979
- .4737	.999	1.008	1.035	.988
- .4211	1.007	1.015	1.046	.998
- .3684	1.013	1.019	1.048	1.007
- .3158	1.014	1.019	1.042	1.012
- .2632	1.011	1.015	1.028	1.014
- .2105	1.005	1.008	1.008	1.012
- .1579	.997	.999	.987	1.007
- .1053	.988	.990	.968	1.001
- .0526	.982	.983	.953	.996
0	.978	.979	.945	.993

REFERENCES

1. R. Gonsalves, Phase retrieval from modulus data, J. Opt. Soc. Am. 66, 961 (1977).

2. R. Barakat and G. Newsam, Numerically stable iterative method for the inversion of wavefront aberrations from measured point spread function data, J. Opt. Soc. Am. 70, 1255 (1980).

3. W.H. Southwell, Wavefront analyzer using a maximum likelihood algorithm, J. Opt. Soc. Am. 67, 396 (1977).

4. D. Youla, Generalized image restoration by the method of alternating orthogonal projections, IEE Trans. Circuits Syst. CAS-25, 694 (1978).

5. A. Papoulis, A new algorithm in spectral analysis and band-limited extrapolation, IEEE Trans. Circuits Syst. CAS-22, 735 (1975).

6. R.P. Boas, Entire Functions (Academic Press, New York, 1954) p. 103.

7. M. Lavrentiev, On Some Improperly Posed Problems of Mathematical Physics (Springer-Verlag, Berlin, 1963).

8. A.N. Tikhonov and V.Y. Arsenin, Solutions of Ill-Posed Problems (Halsted, New York, 1977).

9. C.T. Baker, The Numerical Treatment of Integral Equations (Oxford Univ. Press, Oxford, 1977).

10. G.W. Stewart, Introduction to Matrix Computations (Academic Press, New York, 1973).

11. D. Slepian and H. Pollak, Prolate spheroidal wave functions, Fourier analysis and uncertainty - I, Bell System Tech. J. 40, 43 (1961).

12. H. Landau and H. Pollak, Prolate spheroidal wave functions, Fourier analysis and uncertainty - II, Bell System Tech. J. 40, 84 (1961).

13. W.O. Saxton, Computer Techniques for Image Processing in Electron Microscopy (Academic, New York, 1978) Chap. 5.

14. W.M. Patterson, Iterative Methods for the Solution of a Linear Operator Equation in Hilbert Space - A Survey (Springer-Verlag, Berlin, 1974).

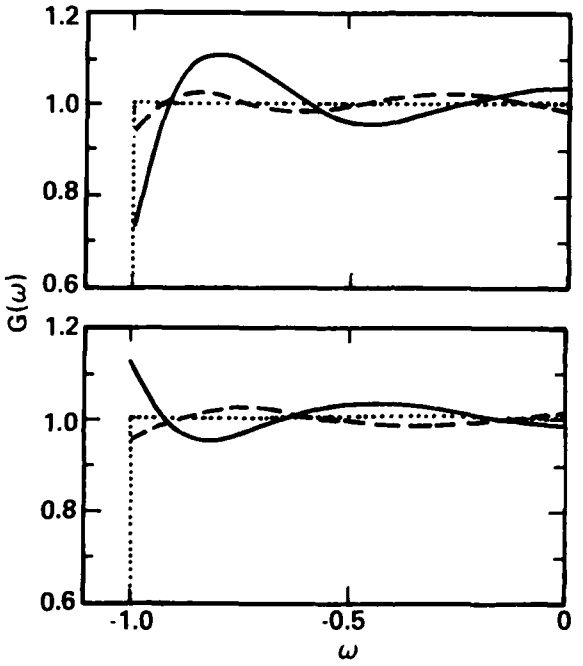

Fig. 1. Four sample realizations of the reconstruction of $G(\omega)$ corresponding to Eq. 4.2 in the presence of 3% noise in $\hat{g}(v)$.

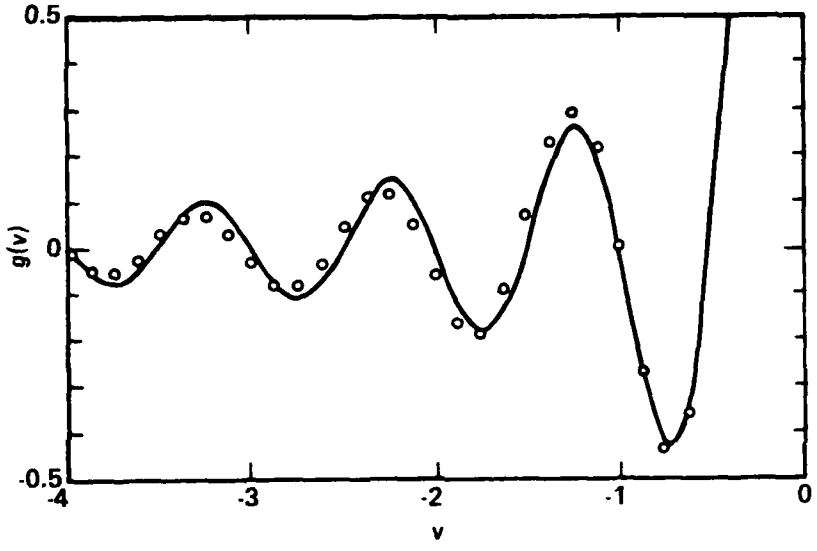

Fig. 2. Extrapolation of g(v), see open circles, corresponding to solid line in upper half of Fig. 1.

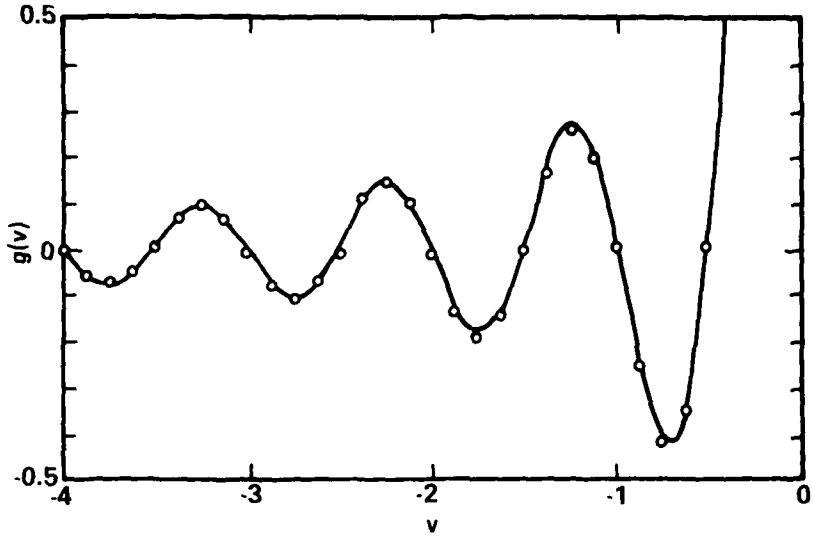

Fig. 3. Extrapolation of g(v), see open circles, corresponding to dashed line in upper half of Fig. 1.

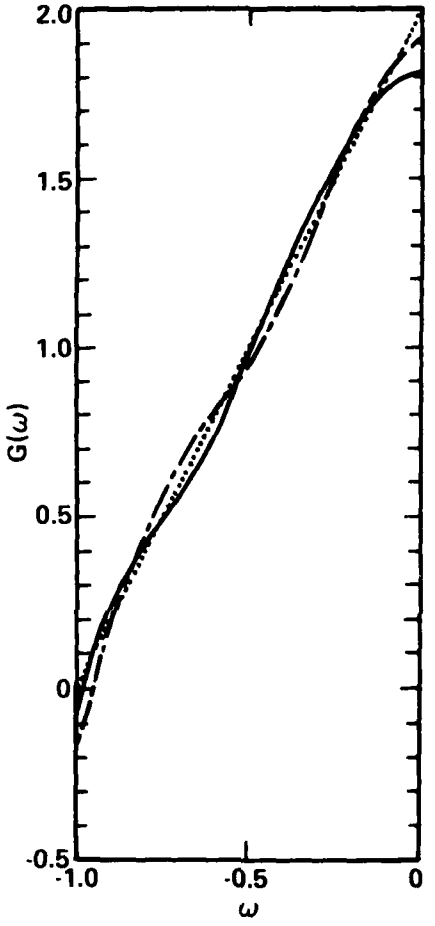

Fig. 4. Two sample realizations (—•— and ——) of the reconstruction of $G(\omega)$ corresponding to Eq. 4.3 in the presence of 3% noise in $\hat{g}(v)$.

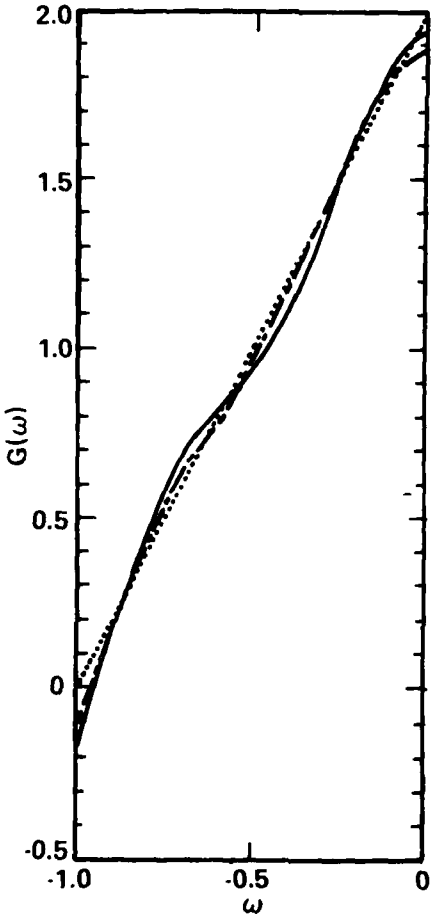

Fig. 5. Two sample realizations (-•- and ——) of the reconstruction of $G(\omega)$ corresponding to Eq. 4.3 in the presence of 3% noise in $\hat{g}(v)$.

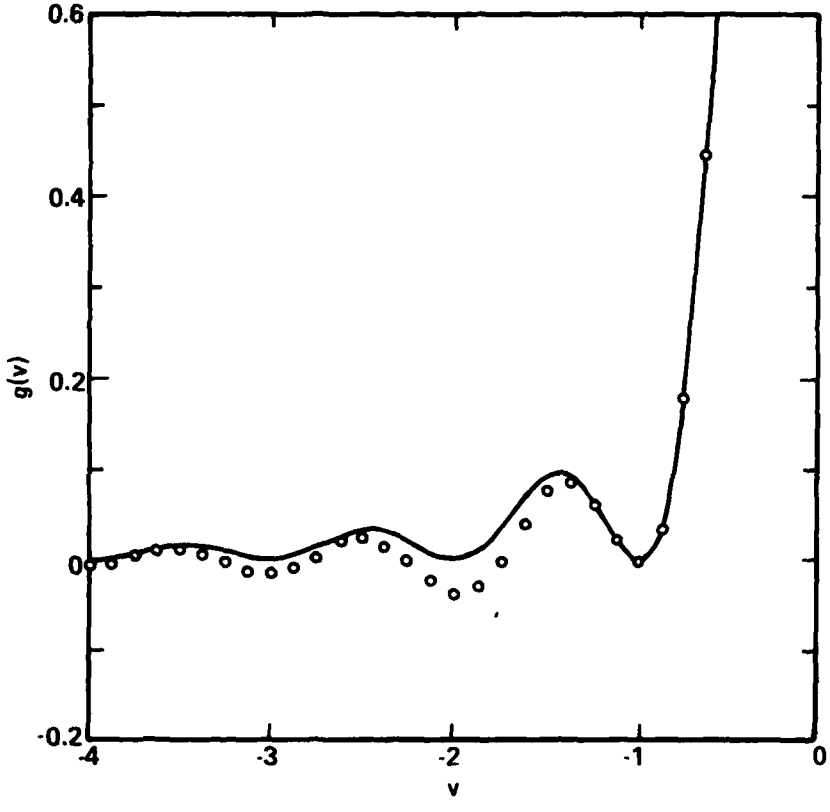

Fig. 6. Extrapolation of g(v), see open circles, corresponding to a noiseless situation.

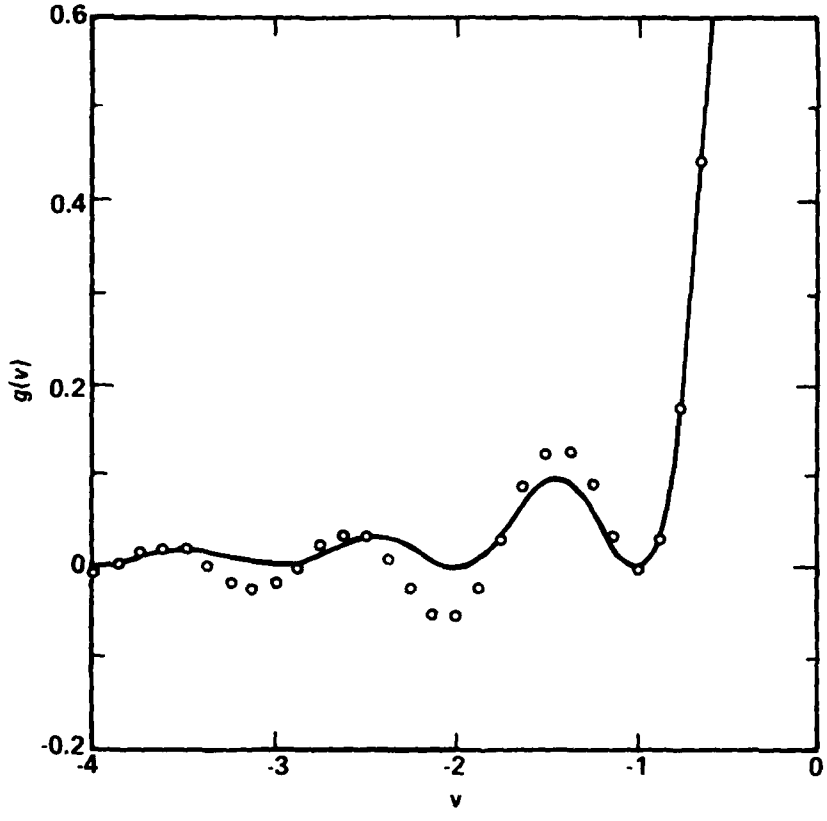

Fig. 7. Extrapolation of g(v), see open circles, corresponding to sample realization (——) in Fig. 4.

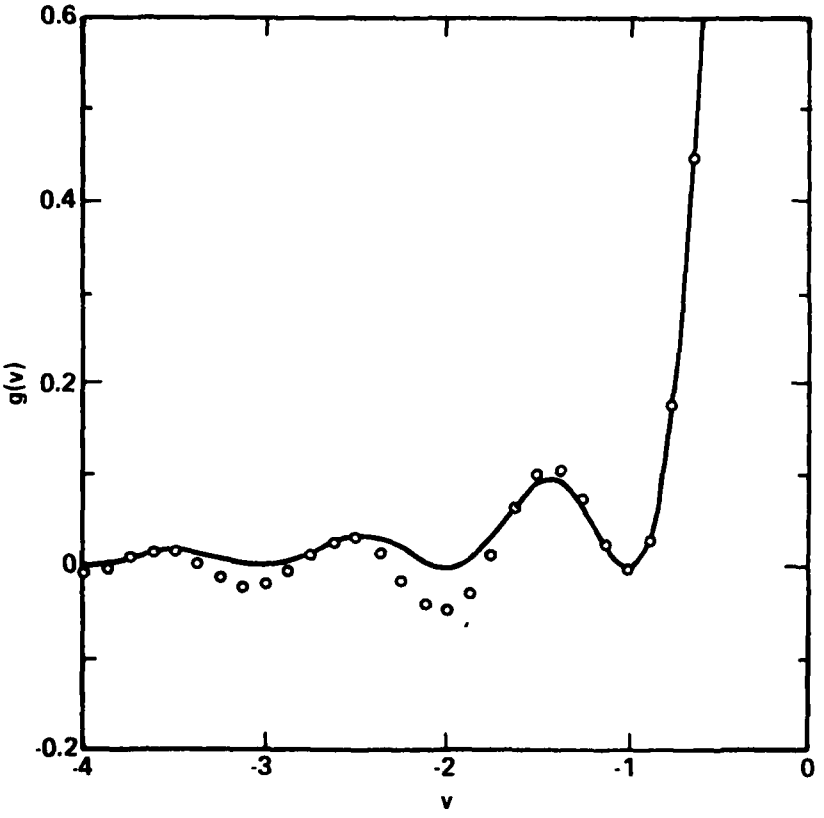

Fig. 8. Extrapolation of g(v), see open circles, corresponding to sample realization (—•—) in Fig. 4.

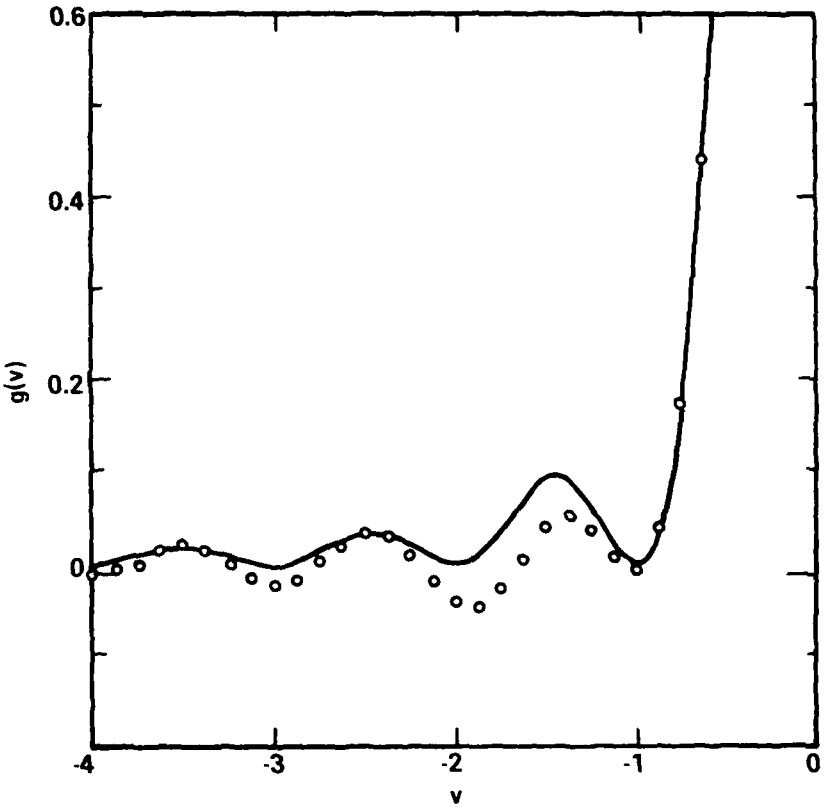

Fig. 9. Extrapolation of g(v), see open circles, corresponding to sample realization (—•—) in Fig. 5.

SECTION 2

INTERFEROGRAM REDUCTION FOR ABERRATED ANNULAR APERTURES VIA ZERNIKE-BARAKAT FUNCTIONS, USING L_2 AND L_1 NORM ALGORITHMS

ABSTRACT

Interferogram reduction of aberrated wavefront data for annular apertures in a hostile environmental is discussed using both the L_2 and L_1 norms.

1. INTRODUCTION

The plan of this section is two-fold. First, the Zernike *functions* appropriate to an annular aperture, as derived by Barakat [1], are briefly summarized. The lower order functions are plotted, discussed, and compared with the Zernike *polynomials* appropriate to an annular aperture. It is concluded that the Zernike *functions* are the natural generalization of the usual Zernike polynomials. Second, the Zernike functions are discussed in the context of interferogram reduction using the usual L_2 norm, commonly termed least squares. However, the L_2 norm is not robust with respect to "outliers" in the raw fringe data such as occur in the hostile environments in which the reduction must be expected to be performed. The L_1 norm is known to be robust with respect to these outliers, and the linear programming approach to solving the overdetermined fringe reduction equations to obtain the aberrated wavefront is discussed.

2. GENERALIZED ZERNIKE FUNCTIONS

The generalized Zernike functions are a set of complete orthogonal functions defined over the annular aperture that were recently introduced by the author [1]. They are conveniently written in cylindrical coordinates as products of angular functions (i.e., trignometric functions) and radial functions. The most general version of the radial functions defined over the annular aperture also contains a bell-shaped amplitude taper; however, we will only concern ourselves with the situation where the amplitude is constant over the unobscured portion of the annular aperture. The radial coordinate of the annular aperture is denoted by ρ with reference to Eq. 2.9 of [1] with $\alpha \equiv 0$, the radial annular functions are

$$B_n^m(\rho,\varepsilon) = N_n^m(\varepsilon)\left(\frac{1-\rho^2}{1-\varepsilon^2}\right)^{\frac{1}{2}} P^{(o,m)}_{(n-m)/2}\left[2\left(\frac{\rho^2-\varepsilon^2}{1-\varepsilon^2}\right)-1\right] \qquad (2.1)$$

where:

ε = obscuration ratio $\quad 0 \leq \varepsilon < 1$

$N_n^m(\varepsilon)$ = normalization factor

$P^{(o,m)}_{(n-m)/2}$ = Jacobi polynomial

Properties of these functions have been obtained by Barakat [*1*] and we refer to this paper for details. Perhaps the most important property is

$$\int_{\varepsilon}^{1} B_n^m(\rho,\varepsilon) B_{n'}^m(\rho,\varepsilon)\, \rho d\rho = h_n^m(\varepsilon)\delta_{nn'}, \tag{2.2}$$

where

$$h_n^m(\rho) = \frac{(1-\varepsilon^2)}{2n+2} \tag{2.3}$$

independent of m. The first few B_n^m functions are listed in Table 1.

Plots of some of the lower order B_n^m functions are shown in Figs. 1 to 5 for an obscuration ration $\varepsilon = .3$; the corresponding Zernike polynomial $R_n^m(\rho)$ is also shown for comparison. In Fig. 6 we show $B_3^1(\rho)$ for $\varepsilon = .5$; compare with Fig. 2. Note that

$$B_n^m(\rho=\varepsilon) = 0 \tag{2.4}$$

just as the regular Zernike polynomials satisfy

$$R_n^m(\rho= 0) = 0 \tag{2.5}$$

In fact, an examination of these curves shows that B_n^m is a scaled version of R_n^m over $\varepsilon \leq \rho \leq 1$. This property is *not* shared by the generalized Zernike *polynomials* introduced originally by Tatian [2] and studied more intensively by Mahajan [3]. It is not our intention to discuss these aspects of the problem here, as we intend to carry out a detailed comparison of the generalized Zernike *functions* and the generalized Zernike *polynomials* in the near future. Nevertheless we have shown in Fig. 6 as the -•- line the corresponding polynomial as explicitly evaluated by Mahajan, which in our notation reads

$$B_3^1(\rho)\big|_{\text{poly}} = \frac{3(1+\varepsilon^2)\rho^3 - 2(1+\varepsilon^2+\varepsilon^4)\rho}{(1+\varepsilon^2-2\varepsilon^4)} \tag{2.6}$$

Note the discontinuous behavior of the polynomial at the edge of the obscured aperture $\rho = .5$.

The generalized Zernike *functions* for the annular aperture are:

$$\zeta_n^m(\rho,\theta) = B_n^m(\rho) \begin{matrix} \cos m \\ \sin m \end{matrix} \tag{2.7}$$

which we abbreviate by letting $\hat{\eta}$ denote ρ,θ so that

$$\zeta_n^m(\hat{\eta}) = \zeta_n^m(\rho,\theta) \tag{2.8}$$

We omit the ε dependence for typographic convenience. In the inversion scheme to be discussed in the next section, it is convenient to employ lexographic ordering of the generalized Zernike functions. They follow naturally into two classes: optical systems possessing rotationally symmetric aberrations, and optical systems lacking any symmetry. The latter are the more important in the context of the problems that we encounter in the deconvolution scheme of things. Thus we now write $\zeta_j(\hat{\eta})$ to denote $\zeta_n^m(\hat{\eta})$ and refer to Tables 2 and 3 for the explicit lexographic ordering employed in the present communication. There is nothing unique about the ordering and one can permute the ordering if desired. The wavefront $W(\hat{\eta})$ for the case of an optical system lacking any symmetry *at a fixed object point* is

$$W(\hat{\eta}) = \sum_{n=0}^{\infty} \sum_{m=0}^{\infty} [c_{mn} \cos m\theta + s_{mn} \sin m\theta] B_n^m(\rho) \qquad (2.9)$$

where c_{mn} and s_{mn} depend upon the object point. The restrictions on n and m are that $n \geq m$ and that (n-m) is an even integer. In the case of an optical system possessing rotational symmetry, s_{mn} vanishes identically. In Table 2 only the cos $m\theta$ terms can appear. In Table 3 both cos $m\theta$ and sin $m\theta$ can appear and the lower case s and c indicate this. For example, j = 14 and

15 both refer to m = n = 4, but j = 14 is associated with cos 4θ while j = 15 is associated with sin 4θ in accordance with Eq. 2.9. We have listed 22 individual aberration terms. Although we can continue to list higher order terms such terms oscillate very rapidly and are of limited use in the diagnostic aspects we shall be studying.

When lexographic ordering is employed, then Eq. 2.9 can be rewritten in the form

$$W(\hat{\eta}) = \sum_{j=1}^{\infty} z_j \, \zeta_j(\hat{\eta}) \tag{2.10}$$

where the expansion coefficients z_j are equivalent to the c and s coefficients in Eq. 2.9.

3. L_1 and L_2 NORM INVERSION SOLUTIONS

The determination of the aberrated wavefront of an optical system is invariably carried out by inverting the fringe systems obtained from interferograms. It is generally assumed that the number of fringe measurements is greater than the number of expansion terms in the *hypothesized* wavefront expansion.

In terms of our problem, the discretized version of Eq. 2.10 becomes (with j→n)

$$\sum_{n=1}^{N} z_n \zeta_m(\hat{\eta}_m) = W(\hat{\eta}_m) \quad , \quad m = 1, 2, \ldots, M \tag{3.1}$$

Where $W_m \equiv W(\hat{\eta}_m)$ is the noisy measured wavefront from the interferometer at the points m = 1, ..., M with $M \geq N$. The unknown expansion coefficients z_n are to be determined.

We can write Eq. 3.1 which is an overdetermined, but possibly rank deficient, system of linear equations in matrix from

$$\hat{\zeta}\hat{z} = \hat{W} \quad . \tag{3.2}$$

Here $\hat{\zeta}$ is M × N (M rows and N columns), $\hat{z}$ the vector of unknowns is N × 1, and $\hat{W}$ the vector of noisy measurements is M × 1.

Our basic problem is to "invert" Eq. 3.2 in order to determine $\hat{z}$ in terms of $\hat{W}$ and $\hat{\zeta}$. In other words, find

the vector of parameters $\hat{z}$ each that Eqs. 3.1 or 3.2 best fits the data. The meaning of the phrase "best fits the data" can be made more precise by defining the residual ($\equiv$ error) term

$$\hat{\varepsilon} \equiv \hat{W} - \hat{\zeta}\hat{z} \tag{3.3}$$

The most common definition for best fit is the L_2 norm criterion, often called the least squares criterion for which $\hat{z}$ is chosen such that

$$\sum_n \varepsilon_n^2 = \text{minimum} \tag{3.4}$$

This procedure dates back to Gauss and Legendre and has been of invaluable use almost since its inception. The standard algorithm amounts to solving the square system

$$\hat{\zeta}^+\hat{\zeta}\hat{z} = \hat{\zeta}^+\hat{W} \tag{3.5}$$

where $\hat{\zeta}^+\hat{\zeta} \equiv$ normal equations. Straightforward application of of this algorithm often involves numerical instabilities that render the "solution" useless such as in lens design where the matrix equivalent of $\hat{\zeta}$ is nearby singular. Fortunately the condition number of $(\hat{\zeta}^+\hat{\zeta})$ defined as [4]

$$C \equiv \frac{\text{largest singular value}}{\text{smallest singular value}} \tag{3.6}$$

is not too large. If C is numerically small, a small relative change in $\hat{\zeta}$ cannot produce a very large relative change in $\hat{z}$ and thus the normal equations are well conditioned. If C has a very small value, then small relative changes in $\hat{\zeta}$ can produce large relative changes in $\hat{z}$ and the normal equations are poorly conditioned. When the normal equations are poorly conditioned the estimate of $\hat{z}$ is a highly unstable function of the observed vector $\hat{W}$. Two slightly different value of $\hat{W}$ will likely produce vastly different values of $\hat{z}$. Fortunately for us the normal equation is relatively well conditioned with large diagonal elements and very small off diagonal elements. This fact follows almost directly from the orthogonality condition Eq. 2.2.

Numerical calculations in the L_2 norm were carried out by using the method of singular value decomposition to evaluate the psuedoinverse. For those readers who are not familiar with the algorithm, reference is made to the standard reference [5] or to Sec. 3 of the interim report RADC-TR-80-154 for details. In the singular value decomposition approach, one completely avoids the normal matrix and deals directly with Eq. 3.2 with generally more accuracy than that achieved by working with Eq. 3.5. Some simulated calculations based upon

synthetic data have been run and the least square/singular value decomposition works extremely well, but this is not really a good test for reasons to be discussed.

The first point concerns the model itself. Now the assumption that the actual wavefront can be fitted by the expansion, Eq. 3.1, is a basic one. In actuality the pupil function of the optical system consists of two terms

$$A(p,q) = A_0(p,q)e^{ikW(p,q)} \tag{3.7}$$

where

$A_0(p,q)$ = amplitude distribution over the exit pupil

$W(p,q)$ = phase distribution (wavefront aberration function measured in wavelength units) over the exit pupil.

The rectangular pupil coordinates p,q are directly related to the cylindrical pupil coordinates ρ,θ. If the amplitude distribution over the exit pupil is constant than the optical system is termed an Airy system. This is the situation we assume to be true when writing down Eq. 3.1. Now if $A_0(p,q)$ varies over the exit pupil in any substantial manner, we have no guarantee that the expansion is a valid representation of the diffraction performance of the optical system in question, even though the curve fit of W is acceptable. The diffraction

performance of an optical system is governed by *both* A_0 and W; only when A_0 is a constant does the determination of W alone become meaningful. Small perturbations of $A_0(p,q)$ from a constant value hopefully have small effects.

Least squares and other inversion techniques have been used for many years to derive best fit models to sets of optical interferometry data; see Malacara's recent text [*6*] for a representative discussion as well as older papers by the author [*7-10*]. It is common practice to test the inversion techniques with synthetic data and to add random noise to the perfect data. The addition of random noise will test the performance of the inversion method in the presence of noise, but it is difficult to determine the influence of the noise on the inverted model parameters. This is because additive noise is unrealistic. Although it is true that many forms of noise encountered in optical interferometry are additive in some sense much of this can be removed by careful instrumentation (and by averaging of repeated measurements in some cases). Noise in the measured wavefront data consists of two types, regardless of how the noise was generated. The first type is that which cannot be fitted to any scalar diffraction model of the wavefront — amplitude over the exit pupil. For

example, if polarization-inducing effects were present they could not be accounted for by scalar calculations in any simple way, although there are ways of handling *some* aspects by a psuedo-scalar approach [*11,12*]. The second type of noise is that which, although it may be unrelated to the actual physics, can be fitted to a scalar diffraction model. The extent to which the expansion parameters in Eq. 3.1 are modulated by this noise is the determining factor as to whether least square formulation is appropriate. This brings us to another question.

This question concerns the quality of the measured noisy data; the presence of residuals (or outliers) of quite unequal sizes calls into question the justification for choosing the fitting to be done by the least squares criterion. In fact, it is well known among statisticians (and virtually unknown to everyone else!) that least square criteria are not very "robust" with respect to outliers in the wavefront fringe data. By "robust" one means that a technique has nearly optimal properties under the standard assumptions and yet remains a good method when various failures of the assumptions occur. Unfortunatley wavefront interferometry is going to be carried out in a hostile environment as regards the active optics that RADC programs contemplate and consequently there will occur

large outliers in the wavefront fringe data over which we will have virtually no control! So that even if we can control the occurrence of large outliers *in a labroatory environment* and thus guarantee the usefulness of the L_2 norm criterion; this happy state of affairs is not the one we have to deal with in using wavefront interferometry for deconvolution because the L_2 norm criterion is too far from the desired robust estimate.

Another possibility is the L_1 criterion (also termed the least absolute deviation) to minimize

$$\sum_n |\epsilon_n| \tag{3.8}$$

This expression is called the L_1 norm of $\hat{\epsilon}$ and the use of this norm is relatively recent although theoretical aspects have been known for a long time [*13*]. A valuable property of the L_1 norm is that it is *robust*

A practical method of solving this type of problem is via the techniques of linear programming. Unfortunately there are no explicit solutions as in the L_2 norm. The linear programming formulation of the L_1 norm problem is:

a. *given* $\hat{\zeta}$ and $\hat{W}$

b. *find*: $\hat{z}$ and the M × 1 vector $\hat{\epsilon}$

which minimize

$$\sum |\epsilon_n| \tag{3.9}$$

subject to

$$\hat{\zeta}\hat{z} + \hat{\epsilon} = \hat{W} \tag{3.10}$$

The problem can be solved in the following fashion. First define the two vectors $\hat{\epsilon}^+$ and $\hat{\epsilon}^-$ (both of which are M × 1) and the two vectors $\hat{z}^+$ and $\hat{z}^-$ as the positive and negative parts of $\hat{\epsilon}$ and $\hat{z}$ respectively. Note that in this subsection the plus sign does not imply that the transpose be taken. Given these remarks we reformulate the above problem as: minimize

$$\sum \hat{\epsilon}^+ + \sum \hat{\epsilon}^- \tag{3.11}$$

subject to

$$\hat{\zeta}(\hat{z}^+ - \hat{z}^-) + \hat{\epsilon}^+ - \hat{\epsilon}^- = \hat{W} \tag{3.12}$$

where

$$\hat{\epsilon}^+, \hat{\epsilon}^- \geq 0, \; z^+, \hat{z}^- \geq 0 \tag{3.13}$$

An efficient numerical program [14] is available for these calculations. We hope to run some realistic simulations in the future.

REFERENCES

1. R. Barakat, Optimum balanced wavefront aberrations for radially symmetric amplitude distributions: generalizations of Zernike polynomials, J. Opt. Soc. Am. 70, 739 (1980).

2. B. Tatian, Aberration balancing in rotationally symmetric lens, J. Opt. Soc. Am. 64, 1083 (1974).

3. V. Mahajan, Zernike annular polynomials for imaging systems with annular pupils, J. Opt. Soc. Am.

4. G. Dahlquist and A. Bjorck, Numerical Methods (Prentice-Hall, Englewood Cliffs, NJ, 1974). p. 176.

5. C. Lawson and R. Hanson, Solving Least Squares Problems (Prentice-Hall, Englewood Cliffs, NJ, 1974). Chap. 7.

6. D. Malaraca, editor, Optical Shop Testing (Wiley, New York, 1978) Appendix 2.

7. R. Barakat, Computation of the transfer function of an optical system from the design data, J. Opt. Soc. Am. 52, 985 (1962).

8. R. Barakat and A. Newman, Measurement of the total illuminance in a diffraction image: point sources, J. Opt. Soc. Am. 53, 1963 (1963).

9. R. Barakat and R. van Ligten, Determination of the transfer function of an optical system from experimental measurements of the wavefront, Appl. Opt. 4, 749 (1965).

10. R. Barakat, General diffraction theory of optical aberration tests from the point of view of spatial filtering, J. Opt. Soc. Am. 59, 1432 (1969).

11. H. Kubota and S. Inoue, Diffraction images in the polarizing microscope, J. Opt. Soc. Am. 49, 191 (1959).

12. R. Barakat, Incoherent diffraction imagery by a polarizing microscope with crossed polarizers, Opt. Acta 27, 847 (1980).

13. J.R. Rice, The Approximation of Functions (Addison-Wesley, Reading, MA, 1964).

14. I. Barrowdale and F. Roberts, Solution of an overdetermined system of equations in the L_1 norm, Comm. A.C.M. 17, 319 (1974).

TABLE 1. LOWER ORDER $B_n^m(\rho,\varepsilon)$

$$B_0^0 = 1$$

$$B_1^1 = (1-\varepsilon^2)^{-1/2}\,(\rho^2-\varepsilon^2)^{1/2}$$

$$B_2^0 = (1-\varepsilon^2)^{-1}\,[2\rho^2-\varepsilon^2-1]$$

$$B_2^2 = (1-\varepsilon^2)^{-1}\,(\rho^2-\varepsilon^2)$$

$$B_3^1 = (1-\varepsilon^2)^{-3/2}\,(\rho^2-\varepsilon^2)^{1/2}\,[3\rho^2-\varepsilon^2-2]$$

$$B_3^3 = (1-\varepsilon^2)^{-3/2}\,(\rho^2-\varepsilon^2)^{3/2}$$

$$B_4^0 = (1-\varepsilon^2)^{-2}\,[3\rho^4-6(1+\varepsilon^2)\rho^2+\varepsilon^4+4\varepsilon^2+1]$$

$$B_4^2 = (1-\varepsilon^2)^{-2}\,(\rho^2-\varepsilon^2)\,[4\rho^2-\varepsilon^2-3]$$

$$B_4^4 = (1-\varepsilon^2)^{-2}\,(\rho^2-\varepsilon^2)^2$$

TABLE 2. LEXOGRAPHIC ORDERING OF THE GENERALIZED ZERNIKE FUNCTIONS FOR ANNULAR APERTURES FOR OPTICAL SYSTEMS POSSESSING ROTATIONALLY SYMMETRIC ABERRATIONS.

j	(m,n)	j	(m,n)
1	(0,0)	6	(1,3)
2	(0,2)	7	(2,2)
3	(0,4)	8	(2,4)
4	(0,6)	9	(3,3)
5	(1,1)	10	(4,4)

TABLE 3. LEXOGRAPHIC ORDERING OF THE GENERALIZED ZERNIKE FUNCTIONS FOR ANNULAR APERTURES FOR OPTICAL SYSTEMS LACKING ANY SYMMETRY IN THE WAVEFRONT.

j	(m,n)	j	(m,n)
1	(0,0)	12	(2,4)c
2	(1,1)c	13	(2,4)s
3	(1,1)s	14	(4,4)c
4	(0,2)	15	(4,4)s
5	(2,2)c	16	(1,s)c
6	(2,2)s	17	(1,s)c
7	(1,3)s	18	(3,5)c
8	(1,3)s	19	(3,5)s
9	(3,3)c	20	(s,s)c
10	(3,3)s	21	(s,s)s
11	(0,4)	22	(0,6)

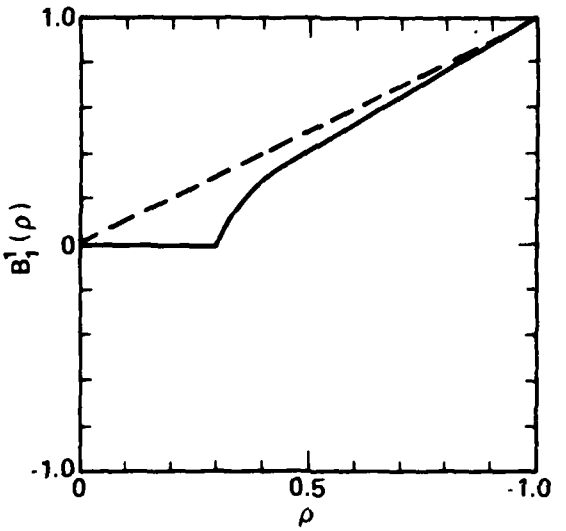

Fig. 1. $B_1^1(\rho)$ for $\varepsilon = .3$ is shown in solid line, $R_1^1(\rho)$ is shown in dotted line.

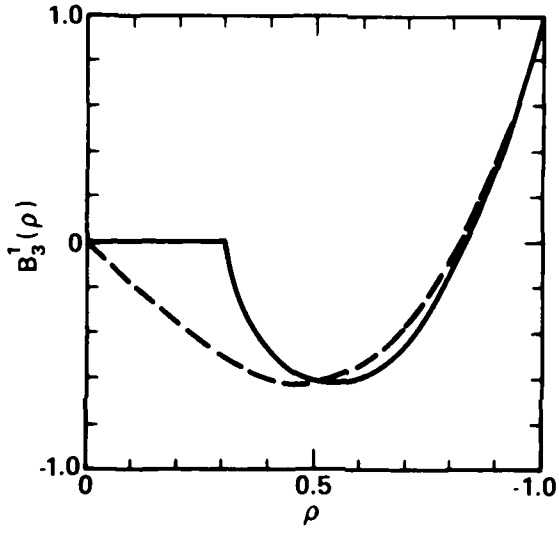

Fig. 2. $B_3^1(\rho)$ for $\varepsilon = .3$ is shown in solid line, $R_3^1(\rho)$ is shown in dotted line.

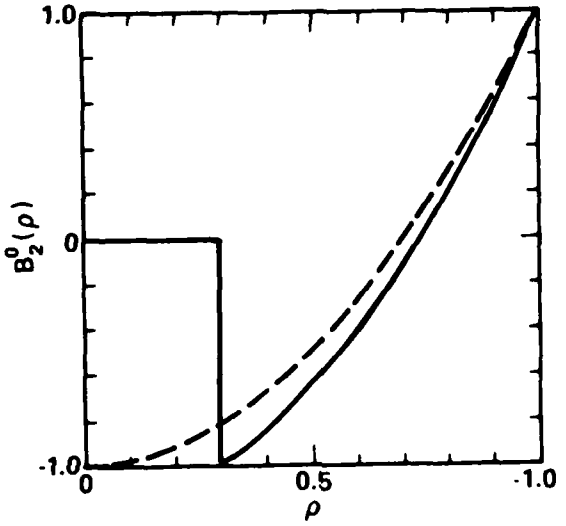

Fig. 3. $B_2^0(\rho)$ for $\varepsilon = .3$ is shown in solid line, $R_3^1(\rho)$ is shown in dotted line.

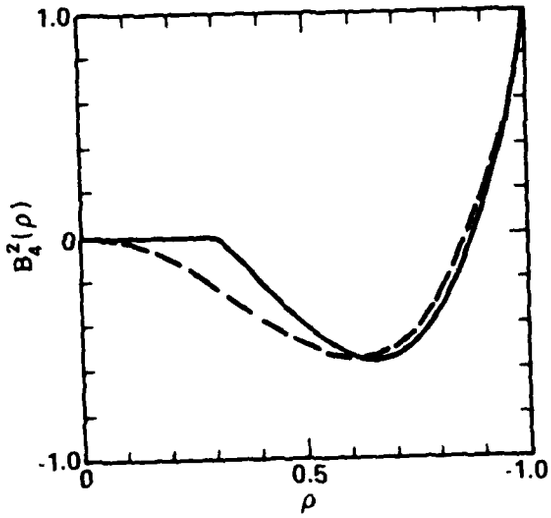

Fig. 4. $B_4^2(\rho)$ for $\epsilon = .3$ is shown in solid line, $R_4^2(\rho)$ is shown in dotted line.

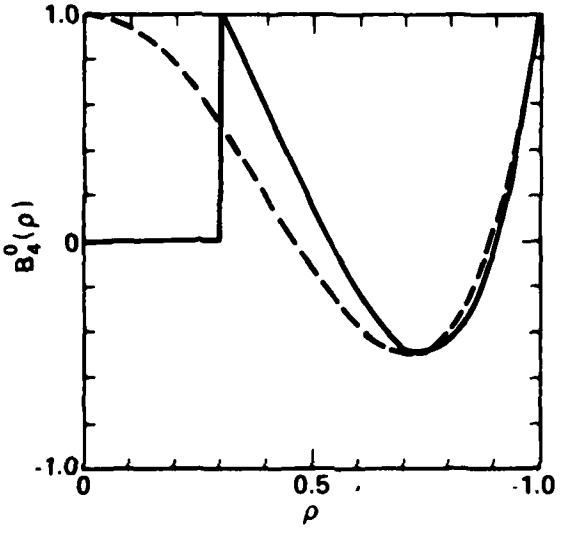

Fig. 5. $B_4^0(\rho)$ for $\varepsilon = .3$ is shown in solid line, $R_4^0(\rho)$ is shown in dotted line.

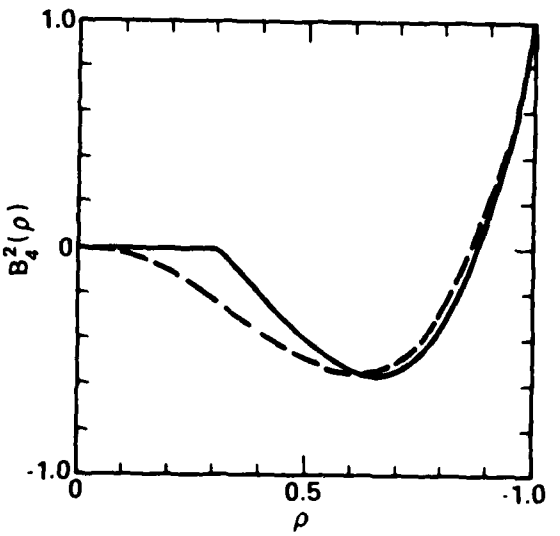

Fig. 6. $B_3^1(\rho)$ for ϵ .5 is shown in solid line,
$R_3^1(\rho)$ is shown in dotted line.
The Zernike polynomial, Eq. 2.6, is shown as the
dash-dot line.

SECTION 3

UPPER AND LOWER BOUNDS ON RADIALLY SYMMETRIC OPTICAL TRANSFER FUNCTIONS

ABSTRACT

For an optical system under incoherent imaging situations the conditions of finite aperture and nonnegative point spread function place restrictive bounds on the values of the corresponing optical transfer function. Under the extra condition that the transfer function be radially symmetric, these bounds can be characterized as the eigenvalues of a real symmetric integral operator. In this paper the bounds are calculated first by analytic inequalities that bound the operator norm, then by finding the eigenvalues of a Galerkin approximation to the operator. In contrast to the slit aperture case, the least upper bound and greatest lower bound are found to differ. The pupil functions which achieve these bounds at a given spatial frequency are determined along with the associated transfer functions.

1. INTRODUCTION

For incoherent imaging situations, the point spread function $t(v_x,v_y)$ is nonnegative. Its Fourier transform, the unnormalized optical transfer function $R(\alpha_x,\alpha_y)$

$$R(\alpha_x,\alpha_y) = \int_{-\infty}^{\infty}\int t(v_x,v_y)\exp(i\alpha_x v_x + i\alpha_y v_y)d\alpha_x d\alpha_y \tag{1.1}$$

has compact support in the α_x,α_y plane that is twice the size of the aperture of the optical system. This follows directly from the fact that $R(\alpha_x,\alpha_y)$ is also the two-dimensional convolution of the pupil function of the optical system [1].

These two requirements place constraints on the behavior of $R(\alpha_x,\alpha_y)$. *The first, that* $R(\alpha_x,\alpha_y)$ *be a positive definite* function (i.e., have a nonnegative Fourier transform) gives the well known results

$$|R(\alpha_x,\alpha_y)| \leq R(0,0) \tag{1.2}$$

$$R(\alpha_x,\alpha_y) = R^*(-\alpha_x,-\alpha_y) \tag{1.3}$$

The second, that $R(\alpha_x,\alpha_y)$ has bounded support, enables calculation of a function $\lambda^+(\alpha_x,\alpha_y)$ such that

$$|R(\alpha_x,\alpha_y)| \leq \lambda^+(\alpha_x,\alpha_y)R(0,0) \tag{1.4}$$

The first such calculation of λ^+ was done by Boas and Kac [2,3] where they derive the least upper bound for the one-dimensional problem of a slit aperture on [-1,+1]

$$\lambda^+(\alpha_x) = \cos \frac{\pi}{\left[2/|\alpha_x|\right]+1} \quad , \quad |\alpha_x| \leq 2 \tag{1.5}$$

where

$$[2/|\alpha_x|] \equiv \text{least interger not less than } 2/|\alpha_x| \tag{1.6}$$

and describe functions that achieve this bound. Although their papers do not mention any physical applications, Professor Kac in a private conversation with one of us (R.B.) remarked that the analysis was done in connection with radar antenna design at the MIT Radiation Laboratory during World War II. This bound was independently derived by Lukósz [4,5] using linear system theory.

A similar result holds in higher dimensions. Suppose a bounded aperture A satisfies the condition that if

$$\hat{p} \equiv (p_1, p_2, \cdots, p_n) \epsilon A \tag{1.7}$$

then the aperture contains the n-dimensional rectangle whose vertices are the points

$$\hat{q} \equiv (\pm p_1, \pm p_2, \cdots, \pm p_n) \tag{1.8}$$

It follows that

$$|R(\hat{\alpha})| \leq \lambda^{+}(\hat{\alpha})R(\hat{0}) \tag{1.9}$$

where

$$\lambda^{+}(\hat{\alpha}) = \cos \frac{\pi}{[2/\sigma]+1}, \quad \sigma > 0 \tag{1.10}$$

and $(2/\sigma)\hat{\alpha}$ lies on the boundary of A. The proof is too lengthy for full reproduction, but its outline is as follows. First, the result is shown for n-dimensional rectangles centered at the origin. Next, a sequence of these rectangles is imbedded inside A such that the rectangles are centered on the origin, have their major axis in the direction $\hat{\alpha}$, and contain the point $(2/\sigma)\hat{\alpha}$ in their limit. Given this construction, it is possible to show that a least upper bound for such a sequence must be a least upper bound for all pupil functions over A, and that the least upper bound for the sequence is Eq. 1.9.

In practice, additional constraints can be imposed on $R(\hat{\alpha})$; in particular by requiring symmetries in the point spread function $t(\hat{v})$. In reference [2] it is shown that the requirement that $t(\hat{v})$ be even does not lower the bounds in Eq. 1.5. Lukosz [5], shows that on a square aperture the requirement of symmetry on the pupil function A(p,q) (where p,q represent the exit pupil coordinates of the aperture) in either the p or q axis, or in both, leads to the same improvement

$$\lambda^{+}(\alpha_x,\alpha_y) \geq \cos \frac{\pi}{[2/|\alpha_x|]+1} \cos \frac{\pi}{[2/|\alpha_y|]+1} \qquad (1.11)$$

where $|\alpha_x|, |\alpha_y| \leq 2$.

In this paper the case of a circular aperture with radially symmetric pupil function

$$A(p,q) \equiv A(\rho) \ , \ \rho = (p^2+q^2)^{\frac{1}{2}} \ , \ o \leq \rho \leq 1 \qquad (1.12)$$

is considered. Obviously the unnormalized transfer function now becomes

$$R(\alpha_x,\alpha_y) \equiv R(\omega), \ \omega = (\alpha_x^2+\alpha_y^2)^{\frac{1}{2}} \ , \qquad o \leq \omega \leq 2 \qquad (1.13)$$

Frieden [6] gives some numerical estimates of λ^{+} for this case; we supplement this work with some analytical bounds. Furthermore using a different numerical procedure outlined in Section 4, we demonstrate that in this case the greatest lower bounds and least upper bounds are *different*. This contrasts with the other cases discussed above, where it was shown that functions $R^{+}(\hat{\alpha}), R^{-}(\hat{\alpha})$ could be found such that [2]

$$R^{+}(\hat{\alpha}) = \lambda^{+}(\hat{\alpha})R(\hat{0})$$

$$R^{-}(\hat{\alpha}) = -\lambda^{+}(\hat{\alpha})R(\hat{0}) \qquad (1.14)$$

Radial symmetry implies that $t(\hat{v})$ is even as well as real so both $R(\omega)$ and $A(\rho)$ are real. This symmetry and Eq. 2.6 show that the ratio $R(\omega)/R(0)$ is the Rayleigh quotient [7] of a real symmetric operator. Thus the extrema λ_ω^+ and λ_ω^- of the quotient, where

$$\lambda_\omega^- \leq \frac{R(\omega)}{R(0)} \leq \lambda_\omega^+ \tag{1.15}$$

have the alternative characterization of being eigenvalues of a symmetric operator (see Eq. 2.9). We use this property in estimating λ_ω^+ and λ_ω^-. The radial symmetry situation is intrinsically different from the previous cases because the transfer function must now satisfy a symmetric integral equation of the second kind. In contrast, the equation similar to Eq. 2.9 derived for a slit aperture in [2] by the calculus of variations is a continuous algebraic equation

$$\begin{aligned} 2\lambda A(\rho) &= A(\alpha-\rho)+A(\alpha+\rho) , \quad |\rho| \leq 1 \\ &= 0 , \quad |\rho| > 1 \end{aligned} \tag{1.16}$$

2. PRELIMINARIES

Let $A(\rho)$ denote the radially symmetric real-valued pupil function over the circular aperture. The unnormalized transfer function $R(\omega)$ can be written in the form [6,8]

$$R(\omega) = \int_0^1 A(\rho)\rho d\rho \int_0^{2\pi} A(q)d\theta \ , \ 0 \leq \omega \leq 2$$

$$= 0 \qquad , \text{elsewhere} \tag{2.1}$$

where

$$q^2 \equiv \omega^2+\rho^2-2\omega\rho\cos\theta \tag{2.2}$$

It will be convenient to abreviate the notation and we write

$$(f,g) \equiv \int_0^1 f(\rho)g(\rho)\rho d\rho \tag{2.3}$$

$$||f||^2 \equiv \int_0^1 f^2(\rho)\rho d\rho \tag{2.4}$$

to denote inner product and associated norm. We also set

$$(K_\omega A)(\rho) \equiv \int_0^{2\pi} A(q)d\theta \tag{2.5}$$

Consequently we can rewrite Eq. 2.1 in the form

$$R(\omega) = \int_0^1 A(\rho)(K_\omega A)(\rho)\rho d\rho = (A,K_\omega A) \tag{2.6}$$

Note that

$$R(0) = 2\pi||A||^2 \tag{2.7}$$

Since the two dimensional convolution of two radially symmetric functions over the circular aperture of unit radius is also symmetric, then K_ω is a self-adjoint operator with respect to the defined inner product. This and Eqs. 2.1, 2.7 imply that $R(\omega)/R(0)$ will be maximized or minimized if and only if $A(\rho)$ is an eigenfunction of K_ω corresponding to the maximum or minimum eigenvalues λ_ω^+ and λ_ω^-, see reference [7]. Thus we solve the homogeneous integral equation

$$\int_0^{2\pi} A(q)d\theta = \lambda_\omega A(\rho) \tag{2.8}$$

or equivalently

$$(K_\omega A)(\rho) = \lambda_\omega A(\rho) \tag{2.9}$$

for the eigenvalues λ_ω^+ and λ_ω^-, along with their corresponding eigenfunctions $A(\rho)$.

In the following sections, various methods for finding λ_ω^+ and λ_ω^- are outlined, along with comments on behavior, performance, etc. of the corresponding eigenfunctions and transfer functions.

3. ANALYTIC BOUNDS

In this section analytic methods are used to bound the modulus of the largest eigenvalue of K_ω using a series of integral inequalities suggested by [9]. K_ω can be written in the normal (symmetrized) form

$$(K_\omega A)(\rho) = 4\int_0^1 k(\omega,\rho,t)tA(t)dt \tag{3.1}$$

where

$$k(\omega,\rho,t) = [4\rho^2t^2-(\omega^2-\rho^2-t^2)^2]^{-\frac{1}{2}}, \quad |\omega-\rho| \leq t \leq \omega+\rho$$

$$= 0 \qquad\qquad , \text{elsewhere} \tag{3.2}$$

Unfortunately

$$\int_0^1 |tk(\omega,\rho,t)|^2dt = \infty \tag{3.3}$$

so that $tk(\omega,\rho,t)$ is not an L_2 kernel; consequently a quick bound on the eigenvalues cannot be established.

Nevertheless, we can proceed in the following fashion by first defining:

$$k_1(\omega,\rho) \equiv \left|\int_0^1 k(\omega,\rho,t)A(t)2tdt\right| \tag{3.4}$$

$$k_2(\omega,\rho) \equiv \int_0^1 |k(\omega,\rho,t)2t|dt \tag{3.5}$$

$$k_3(\omega,t) \equiv \int_0^1 k_2(\omega,\rho)\,|k(\omega,\rho,t)|\,2\rho d\rho \tag{3.6}$$

$$k_4(\omega) \equiv \max_{0\le t\le 1} k_3(\omega,t) \tag{3.7}$$

Since

$$R(\omega) = 2\int_0^1 A(\rho)\rho d\rho \int_0^1 k(\omega,\rho,t)A(t)2tdt \tag{3.8}$$

by virtue of Eq. 2.1, then

$$|R(\omega)| \le 2\left[\int_0^1 A^2(\rho)\rho d\rho\right]^{\frac{1}{2}}\left[\int_0^1 k_1^2(\omega,\rho)\rho d\rho\right]^{\frac{1}{2}} \tag{3.9}$$

by Schwarz's inequality. Furthermore the modulus of $k_1(\omega,\rho)$ can be similarly bounded

$$|k_1(\omega,\rho)| \le \left[\int_0^1 |k(\omega,\rho,t)2t|\,dt\right]^{\frac{1}{2}}\left[\int_0^1 |k(\omega,\rho,t)A^2(t)2t|dt\right]^{\frac{1}{2}} \tag{3.10}$$

These inequalities imply that

$$\begin{aligned}\int_0^1 k_1^2(\omega,\rho)\rho d\rho &\le \int_0^1 k_2(\omega,\rho)\rho d\rho \int_0^1 k(\omega,\rho,t)A^2(t)2tdt \\ &\le \int_0^1 A^2(t)tdt \int_0^1 k(\omega,\rho,t)k_2(\omega,\rho)2\rho d\rho \\ &\le \max_{0\le t\le 1} k_3(\omega,t)\,||A||^2 \end{aligned} \tag{3.11}$$

Upon using Eqs. 2.7 and 3.7, we finally obtain

$$|R(\omega)| \leq [k_4(\omega)]^{\frac{1}{2}} R(0)/\pi \tag{3.12}$$

The function $[k_4(\omega)]^{\frac{1}{2}}/\pi$ was evaluated numerically and appears in the first column of Table 1.

A useful result, found by further use of inequalities on the definition of $k_4(\omega)$, is

$$|\lambda_{\omega}^{+}| \leq \frac{1}{\pi} [k_4(\omega)]^{\frac{1}{2}} \leq \frac{1}{\pi} \arccos \frac{\omega}{2} \tag{3.13}$$

for $\sqrt{2} \leq \omega \leq 2$. Furthermore, Eq. 3.13 is the asymptotically optimal bound in the sense that a sequence of pupil functions $A_{\omega'}(\rho)$ can be constructed that generate extremal transfer functions $R_{\omega'}(\omega)$, such that as $\omega' \to 2$ then

$$\frac{1}{2} \cdot \frac{\arccos(\omega'/2)}{\pi} \leq \frac{R_{\omega'}(\omega=\omega')}{R_{\omega'}(\omega=0)} \leq \frac{\arccos(\omega'/2)}{\pi} \tag{3.14}$$

where

$$\begin{aligned} A_{\omega'}(\rho) &= 0 \ , \ 0 \leq \rho \leq \omega'/2 \\ &= 1 \ , \ \omega'/2 \leq \rho \leq 1 \end{aligned} \tag{3.15}$$

Numerical calculations suggest that the greatest lower bound constant in Eq. 3.14 is not 0.5 but 0.73. These bounds complement the bounds found by Macdonald [8] for $\omega' \to 0$.

4. NUMERICAL METHODS

The second approach tried was a direct calculation of λ_ω^+ and λ_ω^- by appropriate discretization of the integral equation, Eq. 2.9. A finite dimensional Galerkin approximation scheme was used to form a finite dimensional operator approximation $\hat{C}_\omega$ to K_ω.

We first express the pupil function as the finite expansion

$$A(\rho) = \sum_{n=1}^{N} a_n \phi_n(\rho) \ , \ 0 \leq \rho \leq 1 \tag{4.1}$$

The basis functions are

$$\phi_n(\rho) = \left[\frac{2}{\rho_{n+1}^2 - \rho_n^2}\right]^{\frac{1}{2}} \chi_n(\rho) \tag{4.2}$$

where

$$\begin{aligned} \chi_n(\rho) &= 1 \quad \text{if} \quad \rho \varepsilon [\rho_n, \rho_{n+1}] \\ &= 0 \quad \text{if} \quad \rho \notin [\rho_n, \rho_{n+1}] \end{aligned} \tag{4.3}$$

and $\rho_n (n = 1,2,\cdots,N+1)$ is the mesh imposed on $[0,1]$. The $\phi_n(\rho)$ are orthonormal

$$(\phi_n, \phi_m) = \delta_{nm} \tag{4.4}$$

Substitution of Eq. 4.1 into Eq. 2.9 yields

$$\sum_{n=1}^{N} a_n (K_\omega \phi_n)(\rho) = \lambda \sum_{n=1}^{N} a_n \phi_n(\rho) \tag{4.5}$$

Direct use of the orthogonality relation then gives

$$\sum_{n=1}^{N} (\phi_m, K_\omega \phi_n) a_n = \lambda a_m \tag{4.6}$$

where $m = 1,2,\cdots,N$. We can rewrite this in matrix form

$$\hat{C}_\omega \hat{A}_\omega = \mu_\omega \hat{A}_\omega \tag{4.7}$$

where $\hat{C}_\omega$ is a symmetric matrix since $(\phi_m, K_\omega \phi_n) = (\phi_n, K_\omega \phi_m)$. The elements of $\hat{C}_\omega$ could be exactly evaluated since the ϕ_m are piecewise constant functions. *We use μ to denote the eigenvalue of $\hat{C}_\omega$ to distinguish them from the eigenvalues λ of K_ω.*

The Rayleigh quotient corresponding to the symmetric matrix $\hat{C}_\omega$ is [7,10]

$$T(\omega) \equiv (\hat{A}_\omega, \hat{C}_\omega \hat{A}_\omega)/(\hat{A}_\omega, \hat{A}_\omega) \quad . \tag{4.8}$$

Examination of Eqs. 2.6 and 4.8 shows that the Rayleigh quotient can also be written as

$$T(\omega) = \frac{R(\omega)}{R(0)} \tag{4.9}$$

According to a theorem in matrix theory [7,10]

$$\mu_\omega^- \leq T(\omega) \leq \mu_\omega^+ \tag{4.10}$$

where μ_ω^+ is the largest positive eigenvalue of $\hat{C}_\omega$ and μ_ω^- the largest negative eigenvalue and

$$\mu_\omega^+ \equiv \max_{\hat{A} \neq 0} \quad T(\omega) \geq 0$$

$$\mu_\omega^- \equiv \min_{\hat{A} \neq 0} \quad T(\omega) \leq 0 \tag{4.11}$$

Since $\hat{C}_\omega$ is symmetric all eigenvalues are real, but their values must be determined numerically.

The Rayleigh quotient was not calculated directly from Eq. 4.8. Instead a singular value decomposition of $\hat{C}_\omega$ into the form

$$\hat{C}_\omega = \hat{U}\hat{\Sigma}\hat{V}^+ \tag{4.12}$$

was performed, where $\hat{U},\hat{V}$ are orthogonal matrices and $\hat{\Sigma}$ is a diagonal matrix whose entries consist of the absolute values of the eigenvalues of $\hat{C}_\omega$. The theory is detailed in [11], a stable numerical algorithm due to Golub and Reinsch [12] was used for the actual calculations. The signs of elements in $\hat{\Sigma}$ were recovered from the signs of columns of $\hat{U}$ and $\hat{V}$. Since $\hat{C}_\omega$ is symmetric $\hat{U}$ and $\hat{V}$ are identical up to signs on their columns. These in turn determine the signs of the eigenvalues.

The eigenvectors associated with μ_ω^+ and μ_ω^- can now be read off from the columns of $\hat{U}$ or $\hat{V}$ and give an approximation $\hat{A}_\omega$ to the pupil function $A_\omega(\rho)$ that will maximize (or minimize)

$R(\omega)/R(0)$. Calculation of the transfer function associated with $A_\omega(\rho)$ is effected by numerically evaluating the inner product, Eq. 4.8, using the fixed vector $\hat{A}_\omega$, but varying the matrix $\hat{C}_\omega$ corresponding to a variation in its subscript ω over the interval $(0 \leq \omega \leq 2)$.

5. NUMERICAL RESULTS

Using the discretization scheme of section 4, μ_ω^+ and μ_ω^- were calculated using N = 40 in Eq. 4.1. The results are listed in Table 1 and appear in graphical form in Fig. 1. There are four sources of error in μ_ω^+ and μ_ω^- as approximations to λ_ω^+ and λ_ω^-; we discuss them briefly. Round-off errors are negligible since all calculations were done in double precision and the matrices manipulated had relatively small dimension. The choice of basis functions gave closed form expressions for $\hat{C}_\omega$ removing the need to numerically estimate the approximate operator with attendant errors introduced. Various checks run on the singular value decomposition suggested at least 8 figure accuracy in the decomposition, so that error in the decomposition could be disregarded.

The main source of error occurs in approximating K_ω by $\hat{C}_\omega$. Calculations indicated that the error $||K_\omega - \hat{C}_\omega||$ was proportional to 1/N. However, K_ω is a compact operator so it has an infinite sequence of eigenvalues converging on zero, whereas $\hat{C}_\omega$ being finite dimensional has at most N distinct nonzero eigenvalues. Therefore, the relative error of an eigenvalue μ of $\hat{C}_\omega$ as an approximation to an eigenvalue λ of K_ω depends on N *and* the ranking of λ among the eigenvalues of K_ω arranged in absolute value. For all ω, λ_ω^+ has the largest modulus, so is rapidly approximated

by μ_ω^+. For $.5 \leq \omega \leq 2$, λ_ω^- has the second largest modulus and is also well approximated by μ_ω^-. The relative error in both these cases for N = 40 was estimated as less than 0.1%. As $\omega \to 0$, it was observed that $\lambda_\omega^- \to 0$ so that λ_ω^- had a low ranking by absolute value. Thus to achieve a required relative error in μ_ω^- larger N values would be necessary. Nevertheless, for $.1 \leq \omega \leq .5$, N = 40 still gives an estimated error of less than 1%.

In Figs. 2-5, the eigenfunctions $A_\omega^+(\rho)$ and $A_\omega^-(\rho)$ are plotted for some representative values of ω. The associated normalized transfer functions $T(\omega) = R(\omega)/R(0)$ are shown in Figs. 6-9. For $\omega<1$, the eigenfunctions were calculated using an equispaced mesh on [0,1] in Eq. 4.3

$$\rho_n = \frac{1}{N}(n-1) \quad , n=1,\cdots, 41 \tag{5.1}$$

When $\omega>1$, then the kernel $k(\omega,\rho,t)$ in Eq. 3.2 is zero for ρ or t in $[0,\omega-1]$, as these points are no longer in the support of the autocorrelation in Eq. 2.1. Thus, Eq. 2.9 becomes

$$\begin{aligned} \lambda A(\rho) &= (K_\omega A)(\rho), \quad \omega-1 \leq \rho \leq 1 \\ &= 0 \quad , \quad 0 \leq \rho \leq \omega-1 \end{aligned} \tag{5.2}$$

So if $\lambda \neq 0$, then $A(\rho) = 0$ for $\rho \in [0,\omega-1]$. For example, let $\omega=1.2$; then

$$A_{1.2}^+(\rho),\ A_{1.2}^-(\rho) \equiv 0 \text{ for } 0 \leq \rho \leq .2 \tag{5.3}$$

Thus, the optimum pupil functions have variable amplitude annular apertures for $1 \leq \omega \leq 2$. We can take advantage of this fact for $\omega > 1$ by using the following equidistant mesh on $[\omega-1, 1]$

$$\rho_n = (\omega-1) + \frac{1}{N}(2-\omega)(n-1) \tag{5.4}$$

for $n=1,2,\cdots,41$.

Since λ_ω^+ is the largest eigenvalue, then as expected from theory [7], the corresponding eigenfunction $A_\omega^+(\rho)$ will not change sign. As a consequence the corresponding optical transfer function is also one sign (i.e., $T(\omega) \geq 0$, as witness the solid curves in Figs. 6-9). When $\omega \geq .5$, since λ_ω^- is the second largest eigenvalue then $A_\omega^-(\rho)$ will change sign once. However, for $\omega \leq .5$, λ_ω^- has a lower ranking and $A_\omega^-(\rho)$ should oscillate more rapidly. These oscillations in the pupil function induce corresponding oscillations in the transfer function. All these features appear in the graphs.

Frieden [6] obtains value for μ_ω^+ and $A_\omega^+(\rho)$ by expanding $A(\rho)$ in a Fourier-Bessel sampling expansion and maximizing the normalized optical transfer function. His results for μ_ω^+ are in close agreement with our values. His graphs of $A_\omega^+(\rho)$ are also in general agreement with our functions, although his eigenfunctions are much less smooth than ours for $\omega > 1$. This is

because the piecewise constant representation, Eq. 4.1, gives a better resolution of $A_{\omega}^{+}(\rho)$ than the sampling series expansion for $\omega>1$.

REFERENCES

1. M. Born and E. Wolf, Principles of Optics, 4th ed. (Pergamon Press, Oxford, 1970) p. 484.

2. R.P. Boas, Jr. and M. Kac, "Inequalities for Fourier transforms of positive functions," Duke Math. J., 12, 189-206 (1945).

3. R.P. Boas, Jr., "More inequalities for Fourier transforms," Duke Math. J., 15, 105-109 (1948).

4. W. Lukosz, "Properties of linear low pass filters for nonnegative signals," J. Opt. Soc. Am., 52, 827-829 (1962).

5. W. Lukosz, "Uoertragung nicht-negativer signale durch lineare filter," Opt. Acta, 9, 335-364 (1962).

6. B.R. Frieden, "Maximum attainable MTF for rotationally symmetric lens systems," J. Opt. Soc. Am., 59, 402-406 (1969).

7. C.T.H. Baker, The Numerical Treatment of Integral Equations (Oxford Univ. Press, Oxford, 1977) pp. 220-227.

8. J.A. Macdonald, "Apodization and frequency response with incoherent light," Proc. Phys. Soc., 72, 749-756 (1958).

9. K. Yosida, Functional Analysis, 4th ed. (Springer-Verlag, New York, 1974) p. 356.

10. B. Noble and J.W. Daniel, Applied Linear Algebra, 2nd ed. (Prentice-Hall, Englewood Cliffs, NJ, 1977) p. 431.

11. C.B. Moler and G.E. Forsyth, Computer Solutions of Linear and Algebraic Systems (Prentice-Hall, Englewood Cliffs, NJ, 1967) Chpt. 8.

12. G. Golub and C. Reinsch, "Singular value decomposition and least square solutions," Numer. Math., 14, 403-420 (1970).

TABLE 1. BOUNDS ON $T(\omega) \equiv R(\omega)/R(0)$.

ω	$[k_4(\omega)]^{\frac{1}{2}}/\pi$	μ_ω^+	μ_ω^-
0	1.000	1.000	0
.1	1.000	.986	-.357
.2	1.000	.950	-.374
.3	1.000	.896	-.361
.4	1.000	.831	-.339
.5	1.000	.758	-.328
.6	.814	.682	-.285
.7	.714	.605	-.263
.8	.656	.532	-.261
.9	.612	.461	-.242
1.0	.577	.394	-.200
1.1	.354	.343	-.173
1.2	.312	.301	-.153
1.3	.275	.265	-.136
1.4	.243	.232	-.121
1.5	.211	.201	-.106
1.6	.181	.172	-.092
1.7	.151	.143	-.077
1.8	.119	.112	-.061
1.9	.081	.076	-.042
2.0	0	0	0

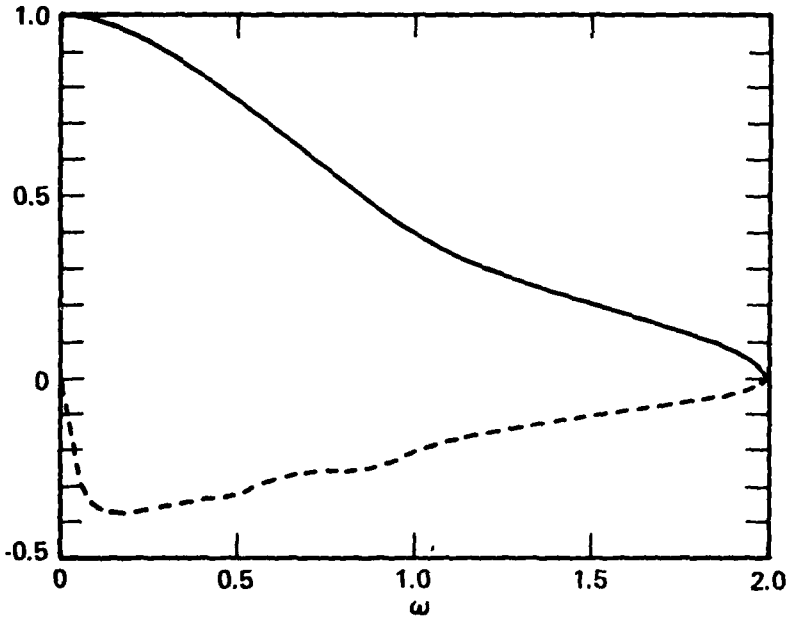

Fig. 1. Approximations μ_ω^+ (——) to upper bound λ_ω^+ and μ_ω^- (– – –) to lower bound λ_ω^- for ratationally symmetric transfer function.

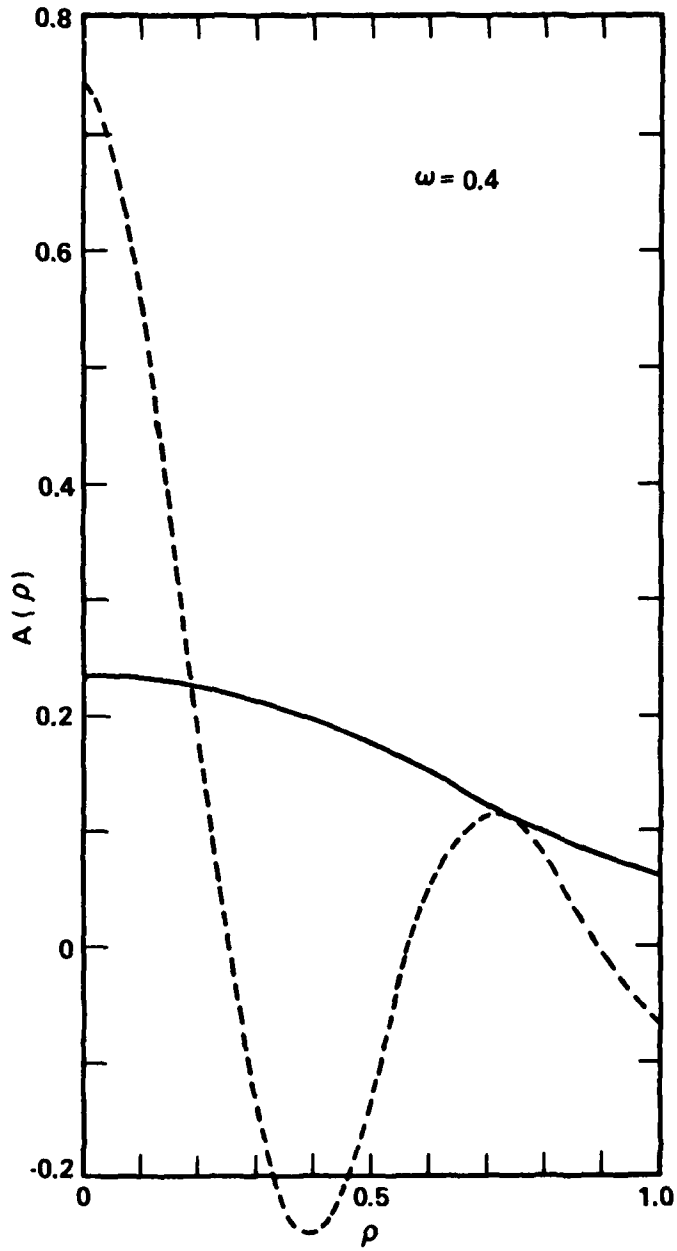

Fig. 2. Pupil functions that achieve the upper bound (——) and lower bound (– – –) at $\omega = .4$.

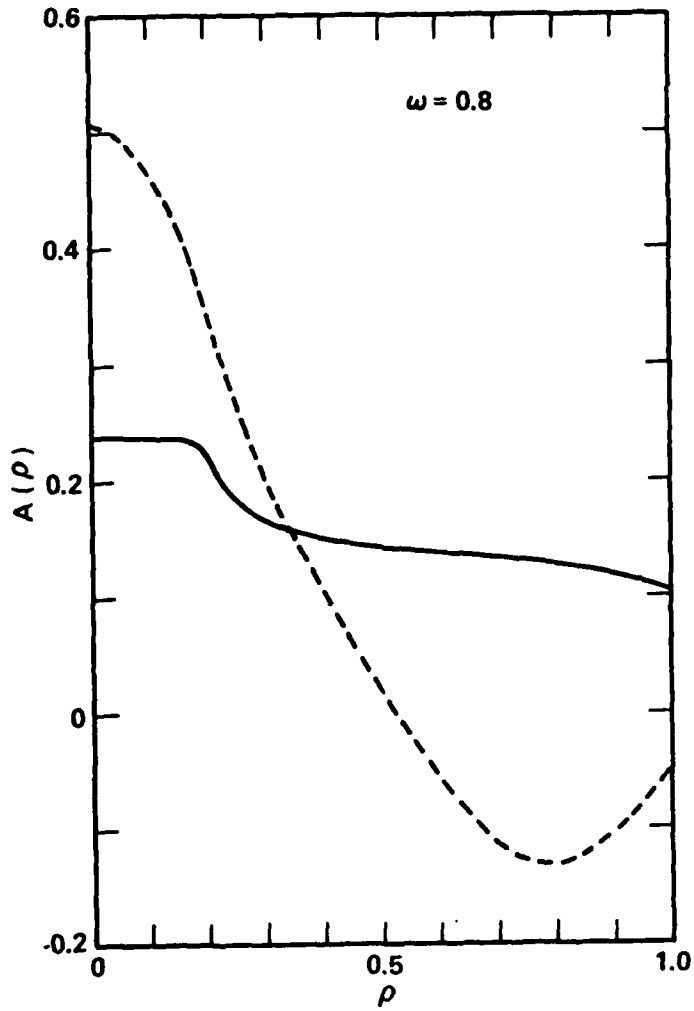

Fig. 3. Pupil functions that achieve the upper bound (——) and lower bound (– – –) at ω = .8.

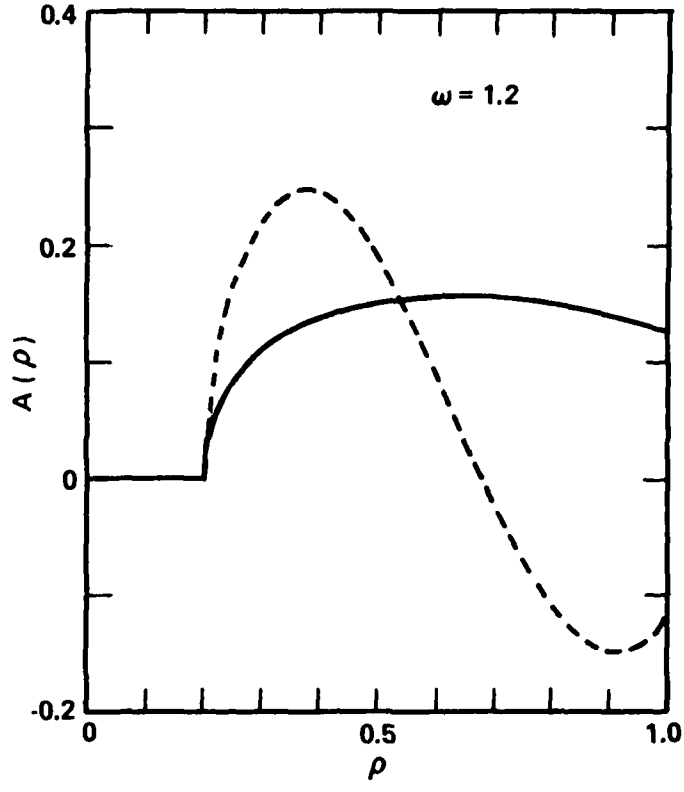

Fig. 4. Pupil functions that achieve the upper bound (——) and lower bound (– – –) at $\omega = 1.2$.

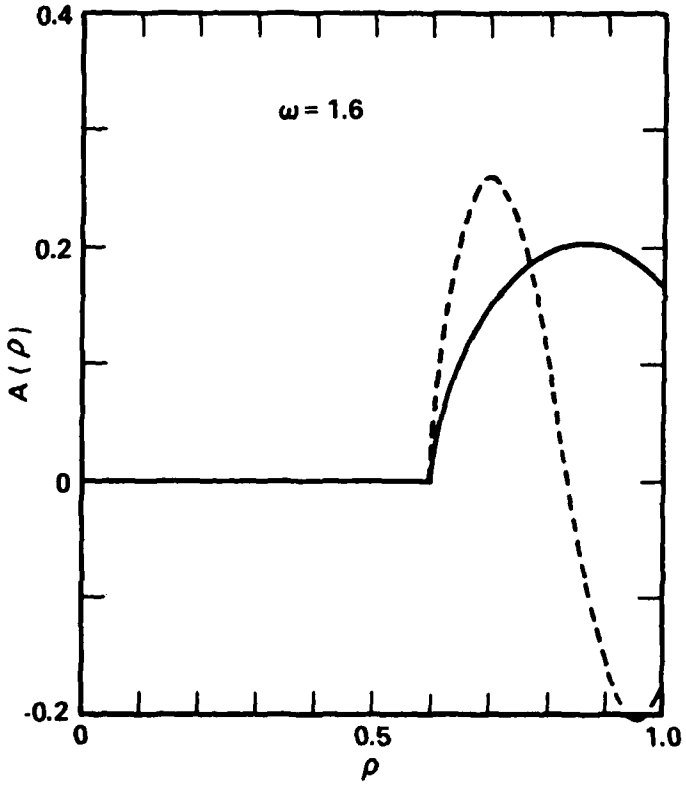

Fig. 5. Pupil functions that achieve the upper bound (——) and lower bound (– – –) at $\omega = 1.6$.

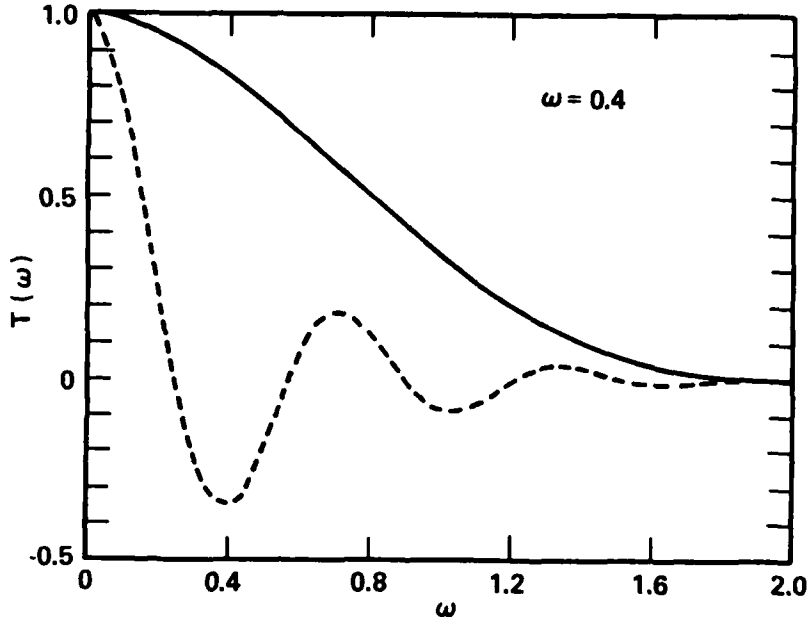

Fig. 6. Optical transfer functions corresponding to data of Fig. 2.

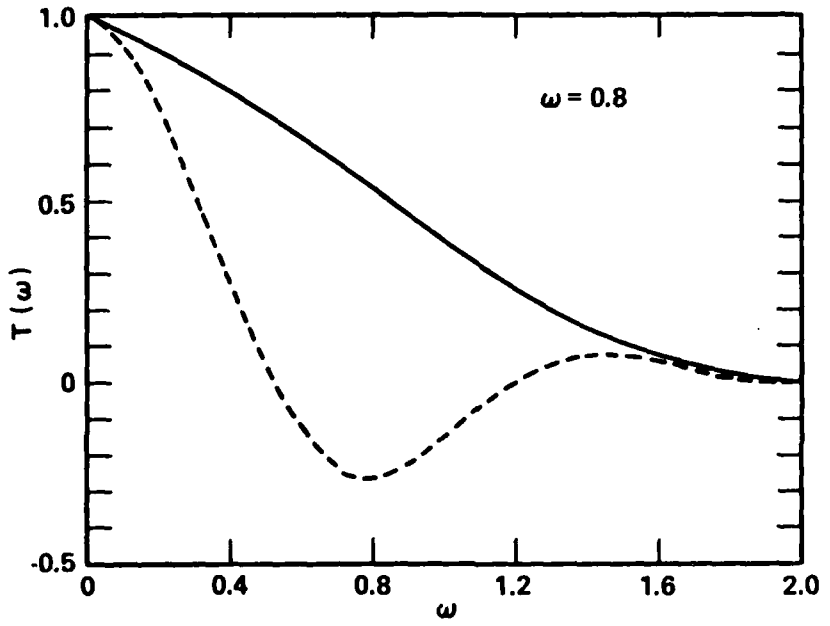

Fig. 7. Optical transfer functions corresponding to data of Fig. 3.

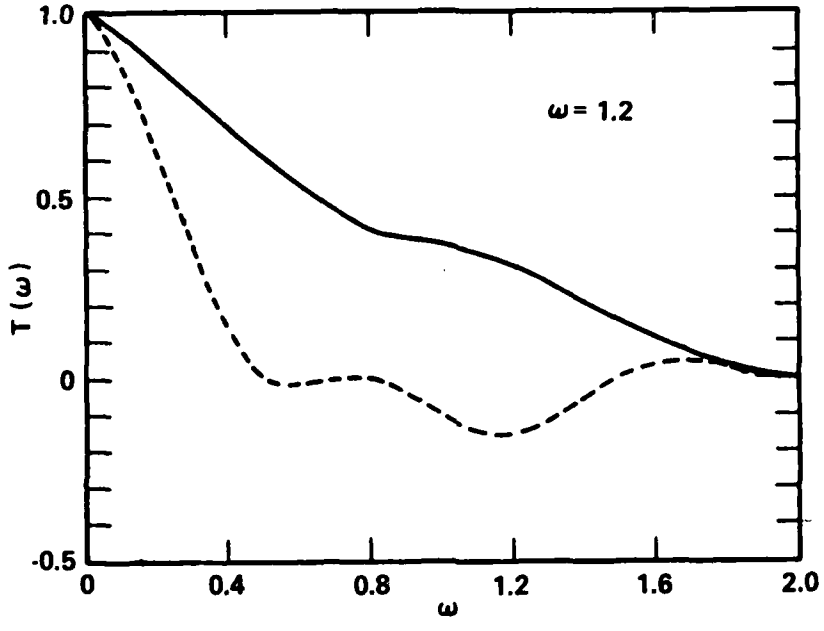

Fig. 8. Optical transfer functions corresponding to data of Fig. 4.

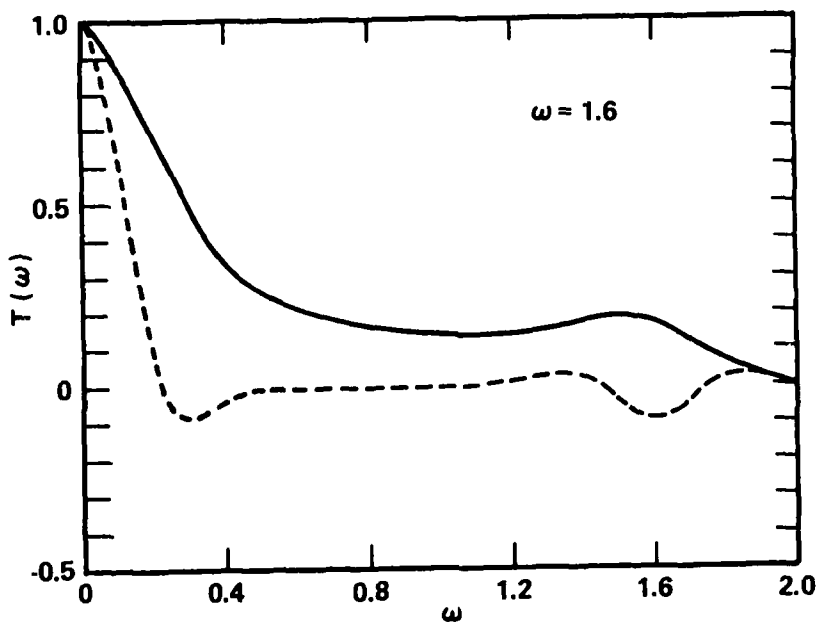

Fig. 9. Optical transfer functions corresponding to data of Fig. 5.

SECTION 4

MOMENT ESTIMATOR APPROACH TO THE RETRIEVAL PROBLEM IN COHERENCE THEORY

ABSTRACT

The purpose of this paper is to suggest a possible approach to the recovery of the spectral density function $g(\omega)$ through a knowledge of the first few measured complex zeros of the complex degree of coherence $\gamma(\tau)$. The assumption that $\gamma(\tau)$ is band-limited allows us to express the sums of inverse powers of the complex zeros of $\gamma(\tau)$ in terms of the moments of $g(\omega)$. Only the lowest-order moments can be evaluated in this manner with any accuracy for reasons discussed in the text. We use two estimation-type solutions that utilize lower-order moments: beta distribution model and the Shannon maximum entropy model to estimate g(CD). Representative numerical calculations are discussed.

Moment estimator approach to the retrieval problem in coherence theory

Richard Barakat

Division of Applied Sciences, Harvard University, Cambridge, Massachusetts 02138
Bolt Beranek and Newman, Inc., Cambridge, Massachusetts 02138

(Received 7 November 1979)

The purpose of this paper is to suggest a possible approach to the recovery of the spectral density function $g(\omega)$ through a knowledge of the first few measured complex zeros of the complex degree of coherence $\gamma(\tau)$. The assumption that $\gamma(\tau)$ is band-limited allows us to express the sums of inverse powers of the complex zeros of $\gamma(\tau)$ in terms of the moments of $g(\omega)$. Only the lowest-order moments can be evaluated in this manner with any accuracy for reasons discussed in the text. We use two estimation-type solutions that utilize lower-order moments: beta distribution model and the Shannon maximum entropy model to estimate $g(CD)$. Representative numerical calculations are discussed.

I. INTRODUCTION

The complex degree of temporal coherence $\gamma(\tau)$ and the spectral density $g(\omega)$ are related by the integral equation[1,2]

$$\gamma(\tau) = \int_0^\infty g(\omega)\, e^{-i\tau\omega}\, d\omega \qquad -\infty < \tau < \infty. \tag{1.1}$$

The spectral density obeys the constraints

$$\text{(a)} \qquad g(\omega) \geq 0, \tag{1.2}$$

$$\text{(b)} \qquad \int_0^\infty g(\omega)\, d\omega = 1 = \gamma(0). \tag{1.3}$$

Considerable efforts along diverse lines have been expended in attempting to invert Eq. (1.1) when only the modulus of $\gamma(\tau)$ is known. The literature on this subject is vast, but some representative references which I have found useful are in-

 0030-3941/80/060688-07$00.50

dicated in Refs. 2-11. As an historical note, it should be mentioned that Akutowicz[12,13] had made a rather complete study of this problem for the L_2 situation, anticipating many subsequent efforts. He was well aware of the physical problem and quoted the x-ray reconstruction problem.

Recently, Napier[14] has been able to measure the first few complex zeros of $\gamma(\tau)$ (see Figs. 3 and 7 of his paper). Napier's very interesting work suggests that a possible approach to the inversion of Eq. (1.1) would be through a knowledge of the first few measured complex zeros of $\gamma(\tau)$.

We briefly outline the approach, leaving the details to the main text. We first assume that the measuring device is a bandpass filter so that there is an upper limit to the possible measured frequencies in Eq. (1.1). This requirement suffices to make $\gamma(\tau)$ an entire function of exponential type when τ is extended to the complex τ plane. An entire function of exponential type has an infinite number of complex zeros; let us call them τ_n. These zeros can be ordered in terms of their moduli so that $|\tau_1| \leq |\tau_2| \leq \cdots$. It is the zeros with the smaller moduli that are measurable.[14] We express the power moments $\langle \omega^n \rangle$ of $g(\omega)$ through the intermediary of the cumulants of $g(\omega)$ in terms of the complex zeros of $\gamma(\tau)$. Although all moments can be evaluated in this manner, only the lowest-order ones can be evaluated from the zeros with any accuracy for reasons discussed in the text. We cannot use the moments of $g(\omega)$ to reconstruct $g(\omega)$ owing to the ill-posed nature of the moment problem.[15,16] Given these considerations, we go to estimation-type solutions that utilize the lower-order moments. We use two such methods, the beta distribution model and the Shannon maximum-entropy model, to estimate $g(\omega)$ in the important case when it is unimodal. Finally, some comments are made on the two-dimensional version of the problem.

II. FORMAL ANALYSIS

To begin we replace the limits in Eq. (1.1) by

$$\gamma(\tau) = \int_a^b g(\omega)\, e^{-i\tau\omega} d\omega \quad 0 \leq |\tau| < \infty, \tag{2.1}$$

where both b and a are finite real numbers. An essential requirement is that b,a are the effective cutoff points in that the integration interval cannot be reduced without altering the value of the integral. $\gamma(\tau)$ is now a band-limited function and by the extended version of the Paley-Wiener theorem[17] is an entire function. As a mathematical note, we will always work in the context of L_2 functions.

There have been several studies of the analytical properties of integrals such as Eq. (2.1), but the most useful for our purposes is that of Titchmarsh.[18] Nussenzveig[6] has listed some of Titchmarsh's theorems that are of relevance to the present application in Sec. III of his paper. The most important theorem is that (in our notation) $\gamma(\tau)$ can be written in the form

$$\gamma(\tau) = e^{-(1/2)(b+a)\tau} \prod_{n=1}^{\infty} (1 - \tau/\tau_n), \tag{2.2}$$

where the product is extended over all the zeros of $\gamma(\tau)$. The product is conditionally convergent. This expression is simpler to use than the usual Hadamard canonical product representation[17,19]

$$\gamma(\tau) = e^{(1/2)(b+a)\tau} \prod_{n=1}^{\infty} [(1 - \tau/\tau_n) e^{\tau/\tau_n}]. \tag{2.3}$$

$\gamma(\tau)$ is hermitian symmetric, $\gamma(-\tau) = \gamma^*(\tau^*)$, because $g(\omega)$ is real. This implies that if τ_n is a zero of $\gamma(\tau)$, then so is $-\tau_n^*$. Thus the distribution of zeros is symmetric with respect to the imaginary τ axis. The non-negativity requirement on $g(\omega)$ further restricts the zeros; obviously, none can now lie upon the imaginary τ axis.

We now take the logarithm of both sides of Eq. (2.2). Since we are working with a complex variable τ, we confine our attention to the principal branch of the logarithm and denote it by Log in conformity with recent usage.[20] Thus for all γ that are not real and negative,

$$\mathrm{Log}\gamma = \mathrm{Log}|\gamma| + i\phi, \tag{2.4}$$

where ϕ is the unique value of $\arg\gamma$ satisfying $-\pi < \phi < \pi$. This is consistent with the convergence test for an infinite product containing complex variables.[20] Thus we have

$$\mathrm{Log}\gamma(\tau) = (1/2)(b+a)(-i\tau) + \sum_{n=1}^{\infty} \mathrm{Log}(1 - \tau/\tau_n). \tag{2.5}$$

The infinite series containing the logarithm can be expanded using

$$\mathrm{Log}\left(1 - \frac{\tau}{\tau_n}\right) = -\sum_{l=1}^{\infty} \frac{1}{l} \left(\frac{\tau}{\tau_n}\right)^l \quad |\tau| < |\tau_1|, \tag{2.6}$$

where the series on the right-hand side converges for all $|\tau| < |\tau_1|$. Substitution of this expression into Eq. (2.5) and subsequent re-summing by changing the order of summation yields

$$\mathrm{Log}\gamma(\tau) = \sum_{n=1}^{\infty} \frac{1}{n!} K_n (-i\tau)^n \quad |\tau| < |\tau_1|. \tag{2.7}$$

The K_n are given by

$$K_1 = (1/2)(b+a) - i \sum_l (\tau_l)^{-1}, \tag{2.8}$$

$$K_n = -i^n (n-1)! \sum_l (\tau_l)^{-n} \quad n \geq 2, \tag{2.9}$$

and are essentially the cumulants associated with $g(\omega)$. The left-hand side of Eq. (2.7) is the second characteristic function[21] extended to the complex τ plane.

Returning to Eq. (2.1), we expand the exponential in the integrand and integrate termwise (which is permissible). The final result is

$$\gamma(\tau) = \sum_{n=0}^{\infty} \frac{1}{n!} \langle \omega^n \rangle (-i\tau)^n, \tag{2.10}$$

where

$$\langle \omega^n \rangle = \int_a^b \omega^n g(\omega)\, d\omega \quad n = 0, 1, \ldots \tag{2.11}$$

are the moments of ω about the origin. These moments always exist and are finite since the limits of integration are finite. The infinite series converges in the entire complex τ plane (i.e., it has an infinite radius of convergence as befits an entire function of exponential type).

The cumulants, in themselves, are of no great intrinsic interest. It is, rather, that they serve as ancillary functions

enabling us to determine the moments in terms of the complex zeros τ_n.

The K_n and $\langle \omega^n \rangle$ are related by a sequence of nonlinear equations that can be obtained from

$$\sum_{n=1}^{\infty} \frac{1}{n!} K_n (-i\tau)^n = \mathrm{Log}\left[1 + \sum_{n=1}^{\infty} \frac{1}{n!} \langle \omega^n \rangle (-i\tau)^n\right], \quad (2.12)$$

where in view of Eq. (2.6), $|\tau| < |\tau_1|$. We simply differentiate both sides with respect to τ and then equate powers of $(-i\tau)$. The first few equations are

$$\begin{aligned} K_1 &= \langle \omega \rangle, \\ \langle \omega \rangle K_1 + K_2 &= \langle \omega^2 \rangle, \\ (1/2)\langle \omega^2 \rangle K_1 + \langle \omega \rangle K_2 + (1/2) K_3 &= (1/2)\langle \omega^3 \rangle. \end{aligned} \quad (2.13)$$

Upon solving for the $\langle \omega^n \rangle$ in terms of the K_n, we have

$$\begin{aligned} \langle \omega \rangle &= K_1, \\ \langle \omega^2 \rangle &= K_2 + K_1^2, \\ \langle \omega^3 \rangle &= K_3 + 3K_2K_1 + K_1^3, \\ \langle \omega^4 \rangle &= K_4 + 4K_3K_1 + 3K_2^2 + 6K_2K_1^2 + K_1^4. \end{aligned} \quad (2.14)$$

It is a well-known property of these functions that the first N cumulants are determined by the first N moments, and *vice versa*. Thus, we have established relations between the moments $\langle \omega^n \rangle$ and the complex zeros τ_n through the intermediary of the cumulants.

Only the first cumulant contains any parameters besides the complex zeros. We can immediately establish the relation

$$i \sum_l (\tau_l)^{-1} = (1/2)(b + a) - \langle \omega \rangle \quad (2.15)$$

by using the first equation in Eq. (2.14). In applications, the limits b and a are known. Furthermore, the mean $\langle \omega \rangle$ can generally be determined by independent means so that we can consider the sum on the left-hand side as known. This is fortunate because, in general, the partial sums of $(\tau_l)^{-1}$ will converge very slowly. Equation (2.15) has already been derived by Titchmarsh,[18] albeit in a different fashion.

Equation (2.15) is important for another reason. The series on the left-hand side is absolutely convergent; as a consequence the complex zeros tend to be located near the real axis for large n. As Nussenzveig[6] has carefully pointed out, it is the zeros located close to the origin that basically determine the shape of $g(\omega)$. The asymptotic distribution of zeros is determined by properties of the cutoff and, consequently, does not contain much information about the shape. We thus expect that the more peaked the spectrum in the interval (a,b), the farther out from the origin will be the zeros.

The reader may well wonder why we do not work *directly* with the infinite product representations of $\gamma(\tau)$ as given by Eqs. (2.2) and (2.3) using a finite number of complex zeros. The reason is simple. Although convergent for all τ, these products are never used for numerical evaluation because the convergence is uniformly slow in any closed set avoiding the complex zeros. Having only a finite number of zeros available simply compounds the problem. These difficulties are well known to numerical analysts.

III. COMMENT ON THE MOMENT PROBLEM

A knowledge of all the moments $\langle \omega^n \rangle$ of $g(\omega)$ suffices to enable one to reconstruct $g(\omega)$. To be somewhat more precise, if the moments of a density function on a *finite* interval are given then they can be used to reconstruct uniquely the unknown density function (this is the Hausdorff moment problem). In the mathematical problem the moments are assumed known to unlimited accuracy. It is tempting to naively apply these considerations to our problem.

Given that we have the *measured* value of the first N complex zeros then we can obtain numerical estimates of all the cumulants. When n is large, only the first zero effectively contributes to the numerical values of the cumulants K_n as defined by Eq. (2.9); consequently,

$$K_n \sim -i^n (n-1)! \tau_1^{-n} \quad n \gg 1. \quad (3.1)$$

Unfortunately, the accuracy of the cumulants suffers in two distinct ways. The lower-order cumulants are in error because a large number of zeros must be known before the series in Eq. (2.9) converges. The higher-order cumulants are in error because, although only a few complex zeros need be known, these measured zeros are raised to very high inverse powers with their attendant inaccuracy. (If τ_1 is in error by 1%, then its *20th* power is in error by 20%.) Errors in the K_n manifest themselves by propagating even larger errors into the $\langle \omega^n \rangle$ via Eq. (2.14). Although we can obtain numerical values for the moments, they are all subject to varying degrees of error.

The moment problem on a finite interval, although determinate, is ill-posed in the sense that very small changes in the moments lead to large changes in $g(\omega)$. Obviously, we cannot usefully employ the Hausdorff procedure to obtain $g(\omega)$ for the type of problem we are discussing.

Given these considerations, we opt for estimation-type solutions that will utilize the lower-order moments (in manners to be specified). In particular, we confine attention to the important case where $g(\omega)$ is unimodal but not necessarily symmetric. We will use two different methods: the beta distribution model and the Shannon maximum entropy model.

IV. ESTIMATION: BETA DISTRIBUTION MODEL

In the beta distribution model, the spectrum is assumed to be of the form

$$g(\omega) = \frac{(\omega - a)^{p-1}(b - \omega)^{q-1}}{B(p,q)(b-a)^{p+q-1}} \quad a \le \omega \le b. \quad (4.1)$$

$B(p,q)$ is the beta function

$$B(p,q) = \Gamma(p)\Gamma(q)/\Gamma(p+q). \quad (4.2)$$

We shall be concerned with the case where the parameters p and q are such that $p > 1$ *and* $q > 1$. Under these circumstances $g(\omega)$ is unimodal and vanishes at the endpoints, i.e., $g(a) = g(b) = 0$. By varying p and q we can obtain a wide variety of shapes in the basic interval $(a \le \omega \le b)$. The mode [value of ω for which $g(\omega)$ is a maximum] is

$$\text{mode} = \frac{(p-1)b + (q-1)a}{p + q - 2}. \quad (4.3)$$

TABLE I. Values of cumulants K_2 and K_4 in terms of first $2N$ zeros of $J_3(\tau)$.

N	K_2	% Error	$-K_4 \times 10^{-2}$	% Error
6	0.09876	21.0	0.92859	0.95
8	0.10417	16.7	0.93304	0.48
10	0.10733	13.8	0.93496	0.27
12	0.11025	11.8	0.93592	0.17
14	0.11213	10.3	0.93645	0.11
16	0.11358	9.1	0.93677	0.08
18	0.11474	8.2	0.93697	0.06
20	0.11568	7.5	0.93710	0.04
∞	0.12500	—	0.93750	—

The moments about the origin are

$$\langle \omega \rangle = \frac{1}{B(p,q)} \sum_{l=0}^{n} \binom{n}{l} (b-a)^{n-l} a^l B(p+l,q). \quad (4.4)$$

The beta density function, Eq. (4.1), is one of a class of probability density functions belonging to the so-called Pearson system of density functions.[22] These density functions are distinguished by the fact that they are determined by the first four moments. The algorithm for determining the four parameters p, q, a, and b in Eq. (4.1) in terms of $\langle \omega \rangle$, ..., $\langle \omega^4 \rangle$ is described in the Elderton and Johnson monograph[22] to which the interested reader is referred for full details. A short summary of the relevant parts of the algorithm is included in the Appendix.

In the calculations that follow, we assume that the mean, $\langle \omega \rangle$, is known from independent measurements. We consider two cases. In the first case, $g(\omega)$ will be symmetric, while in the second it will be nonsymmetric.

In the first situation we take

$$g(\omega) = \frac{(1+\omega)^{\nu-1/2}(1-\omega)^{\nu-1/2}}{2^{\nu} B(\nu+\frac{1}{2}, \nu+\frac{1}{2})} \quad -1 \le \omega \le 1, \quad (4.5)$$

where $\nu > -\frac{1}{2}$ (i.e., $p = q = \nu + \frac{1}{2}$). This function is symmetric about its mode (located at $\omega = 0$). The corresponding $\gamma(\tau)$ is given by[23]

$$\gamma(\tau) = \Gamma(1+\nu) J_{\nu}(\tau)/(\tau/2)^{\nu} \quad \gamma(0) = 1, \quad (4.6)$$

and $\nu > -\frac{1}{2}$. The zeros of $\gamma(\tau)$ are given by the zeros of $J_{\nu}(\tau)$. Now these zeros are real when $\nu > -\frac{1}{2}$, (see Watson[23] for the proof). Following standard notation we denote the *positive* real roots by $j_{\nu,l}$. They are extensively tabulated.[23,24] When the cumulants are expressed in terms of the zeros, we have

$$K_{2n+1} = -(2n)!\, i^{2n+1} \sum_{l=1}^{\infty} [(j_{\nu,l})^{-(2n+1)} + (-j_{\nu,l})^{-(2n+1)}] \equiv 0, \quad (4.7)$$

$$K_{2n} = -(2n-1)!\, i^{2n} 2 \sum_{l=1}^{\infty} (j_{\nu,l})^{-2n} = -2(2n-1) i^{2n} \sigma_{\nu}^{(n)}, \quad (4.8)$$

where

$$\sigma_{\nu}^{(n)} \equiv \sum_{l=1}^{\infty} (j_{\nu,l})^{-2n} \quad (4.9)$$

are the Rayleigh sums.[23] Rayleigh[25] showed that

$$\sigma_{\nu}^{(1)} = \frac{1}{2^2(1+\nu)}, \quad \sigma_{\nu}^{(2)} = \frac{1}{2^4(1+\nu)^2(2+\nu)}. \quad (4.10)$$

Consequently,

$$K_2 = \frac{1}{2\nu+2}, \quad K_4 = \frac{3}{4(\nu+1)^2(\nu+2)}. \quad (4.11)$$

All our calculations will be performed for $\nu = 3$. Values of the cumulants K_2 and K_4 in terms of the first $2N$ zeros, $j_{3,l}$, of $J_3(\tau)$ are listed in Table I. The rate of convergence of the partial sums of K_2 is depressingly slow; $N = 20$ is still 7.5% in error, whereas the corresponding partial sum for K_4 is only 0.04% in error.

Calculations (via the Pearson algorithm) were carried out to estimate ν for values of K_2 and K_4 corresponding to $N = 10$ and $N = 20$. The estimated $g(\omega)$ are

$N = 10$:

$$\hat{g}(\omega) = \frac{(1-\omega^2)^{1.224}}{B(0.5,2.224)} \quad \nu = 1.724;$$

$N = 20$:

$$\hat{g}(\omega) = \frac{(1-\omega^2)^{1.784}}{B(0.5,2.784)} \quad \nu = 2.284;$$

compared with the true $g(\omega)$

$N = \infty$:

$$g(\omega) = \frac{(1-\omega^2)^{2.5}}{B(0.5,3.5)} \quad \nu = 3.000.$$

The results are summarized in Fig. 1. Although the resultant estimates $\hat{g}(\omega)$ are symmetric, they possess a larger variance owing to the fact that the values of $\omega = 0$ are so low.

Generally speaking we have been concerned with the "worst possible" case. Actually, the variance of the original spectrum $g(\omega)$ can usually be measured independently with fair accuracy (say, 3%–5%). Thus, if we take K_2 (the variance) to be 4% in error, thereby effectively halving the error in K_2 for $N = 20$, and repeat the calculations, we obtain

$$g(\omega) = \frac{(1-\omega^2)^{2.110}}{B(0.5,3.110)} \quad \nu = 2.610.$$

The new estimate is shown in Fig. 2 and does not require any detailed comment.

For our second example, we take

$$g(\omega) = \omega^{p-1}(1-\omega)^{q-1}/B(p,q) \quad 0 \le \omega \le 1. \quad (4.12)$$

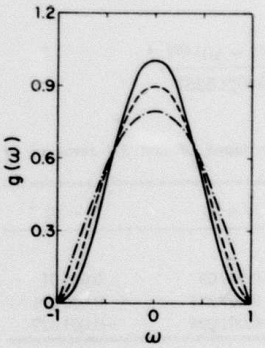

FIG. 1. Beta spectrum with $\nu = 3$ and estimates: ——— exact spectrum; - - - $N = 10$; · · · $N = 20$.

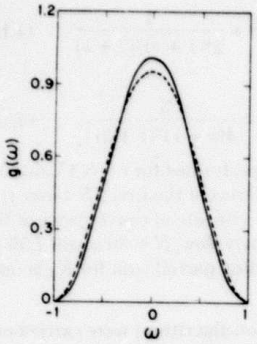

FIG. 2. Beta spectrum with $p = 3$: ——— exact spectrum; - - - modified estimate with $N = 10$.

We let $p = 2, q = 3$ in the numerical calculations. According to Eq. (4.3), the mode is located at $\omega = 1/3$ and the curve is asymmetric. The function $\gamma(\tau)$ corresponding to this expression is

$$\gamma(\tau) = M(p,p+q,-i\tau), \tag{4.13}$$

where $M(a,c;x)$ is the confluent hypergeometric function.[26] In our particular case,

$$\gamma(\tau) = M(2,3,-i\tau)$$
$$= 2(i\tau)^{-2}\int_0^{i\tau} xe^{-x}dx, \tag{4.14}$$

by virtue of Eq. (VI) on p. 46 of Ref. 26. Consequently,

$$\gamma(\tau) = 2(i\tau)^{-2}[1-(i\tau)e^{-i\tau}-e^{-i\tau}]. \tag{4.15}$$

The complex zeros of this function were evaluated using the algorithm developed by Delves and Lyness[27] to locate and compute all the zeros of a given analytic function that lie in a given region. It might be said that this is a complicated problem. Nevertheless, we know the theoretical values of the cumulants; they are

$$K_1 = 2/5, \quad K_2 = 1/25, \quad K_3 = 2/875, \quad K_4 = 9/8750. \tag{4.16}$$

The relevant data is summarized in Table II.

Calculations were again carried out to estimate p and q for values of the cumulants corresponding to $N = 10$ and $N = 20$ of Table II. The estimated $g(\omega)$ are

$N = 10$:

$$\bar{g}(\omega) = \frac{\omega^{0.241}(1-\omega)^{0.887}}{B(1.241,1.887)};$$

$N = 20$:

$$\bar{g}(\omega) = \frac{\omega^{1.040}(1-\omega)^{1.828}}{B(2.040,2.828)}.$$

TABLE II. Values of cumulants in terms of first $2N$ zeros of $M(2,3,-i\tau)$.

	Exact	$N = 20$	$N = 10$
K_1	0.4	—	—
K_2	0.04	0.037 09	0.035 01
K_3	0.002 286	0.002 237	0.002 191
K_4	−0.001 029	−0.001 028	−0.001 027

These estimates are plotted along with the true $g(\omega)$ in Fig. 3. The estimated $\bar{g}(\omega)$ corresponding to $N = 10$ leaves something to be desired, however; that for $N = 20$ is, in my opinion, very reasonable. As before, this is "worst case." When we take K_2 to have a 4% error corresponding to an independent measurement, then the new estimate is

$$\bar{g}(\omega) = \frac{\omega^{1.042}(1-\omega)^{2.103}}{B(1.042,2.103)}.$$

Although we will not plot this estimate, it is very close to the true $g(\omega)$.

V. MAXIMUM ENTROPY SOLUTION

Given that we have numerical estimates of the first N moments, we wish to employ this information to approximate $g(\omega)$ without the intervention of an assumed $g(\omega)$ as in Sec. IV. Following Shannon[28] and Jaynes,[29] we seek the minimally prejudicial assignment of $g(\omega)$ by maximizing its entropy

$$H = -\int_a^b g(\omega)\log[g(\omega)]\,d\omega \tag{5.1}$$

subject to the power-moment constraints

$$\langle\omega^n\rangle \equiv \int_a^b \omega^n g(\omega)\,d\omega \quad n = 1,\ldots,N, \tag{5.2}$$

where the $\langle\omega^n\rangle$ are given.

This is a standard problem in the calculus of variations. The *formal* solution is

$$\bar{g}(\omega) = g_0 \exp\left(-\sum_{n=1}^{N}\lambda_n\omega^n\right), \tag{5.3}$$

where λ_n are the unknown Lagrange multipliers and g_0 is a normalizing constant such that Eq. (1.3) is satisfied. The λ_n are required to satisfy the constraints that the first N moments of $\bar{g}(\omega)$ equal the first N moments of $g(\omega)$. This leads to N simultaneous nonlinear equations for the λ_n. These equations can be solved by Newton-Raphson iteration. We omit the details.

Some numerical calculations have been carried out to test this estimation algorithm. The results cannot be said to be as useful as one would hope for. One of the main difficulties is that $\bar{g}(a) \neq 0$ and $\bar{g}(b) \neq 0$. This causes a severe distortion

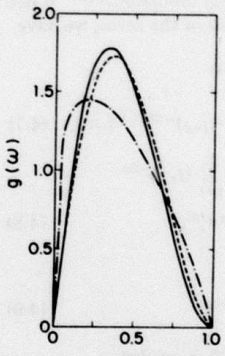

FIG. 3. Nonsymmetric beta spectrum and estimates: ——— exact spectrum; - - - $N = 10$; - - - $N = 20$.

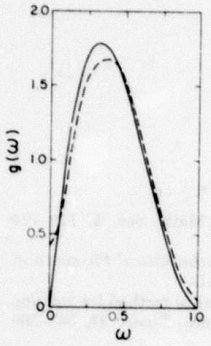

FIG. 4. Nonsymmetric beta spectrum: ——— exact spectrum; - - - maximum entropy estimate given exact moments.

of the estimated $g(\omega)$. For example, $g(\omega)$ given by Eq. (4.12) was numerically tested assuming that the exact values of the cumulants (and hence the moments) are given by Eq. (4.16). The result of such a calculation using maximum entropy is given in Fig. 4. The estimated curve, *given the exact moments*, is in error owing to the nonzero behavior at the endpoints. Calculations with data given in Table II were even worse!

A modification of the algorithm to require the *a priori* constraints $\bar{g}(a) = \bar{g}(b) = 0$ would probably improve the situation, at the cost, although, of an even more involved algorithm. We hope to undertake these modified calculations in the near future.

VI. COMMENT

It is tempting to generalize these results to the two- (or more) dimensional problem

$$\gamma(\tau_1,\tau_2) = \int_a^b \int g(\omega_1,\omega_w) e^{-i\tau_1\omega_1 - i\tau_2\omega_2} d\omega_1 d\omega_2. \quad (6.1)$$

However, no straightforward generalization is possible. When $\gamma(\tau_1,\tau_2)$ is considered as a function of *two* complex variables, then it is an entire function of these two variables as discussed in Ronkin.[30] The difficulty is that $\gamma(\tau_1,\tau_2)$ does not possess any kind of Hadamard factorization because the zeros of $\gamma(\tau_1,\tau_2)$ are not completely discrete. The zeros can form a manifold of values.[30] Consequently we cannot express the cumulants in terms of simple sums of inverse powers of the complex zeros.

ACKNOWLEDGMENTS

I wish to thank Professor Stanley Robinson of the Air Force Institute of Technology for several stimulating conversations. This work was supported in part by the Rome Air Development Center.

APPENDIX

The beta spectrum, Eq. (4.1), contains four parameters: a, b, p, and q. The procedure for determining these parameters is to equate the sample and population values of the first four moments and to solve these four simultaneous nonlinear equations for the four unknown parameters. Now the sample values of the first four moments, Eqs. (2.14), are expressed directly in terms of the cumulants.

The recipe is as follows: First calculate the parameters β_1 and β_2 from the sample moments:

$$\beta_1 = \langle(\omega - \langle\omega\rangle)^3\rangle^2 / \langle(\omega - \langle\omega\rangle)^2\rangle^3, \quad (A1)$$

$$\beta_2 = \langle(\omega - \langle\omega\rangle)^4\rangle / \langle(\omega - \langle\omega\rangle)^2\rangle^2. \quad (A2)$$

β_1 measures the skewness and β_2 the "flatness" of $g(\omega)$. Both of these parameters can be written in terms of the cumulants; in fact,

$$\beta_1 = K_3^2/K_2^3, \quad (A3)$$

$$\beta_2 = (K_4 + 3K_2^2)/K_2^2. \quad (A4)$$

Next, calculate

$$r = 6(\beta_2 - \beta_1 - 1)/(6 + 3\beta_1 - 2\beta_2). \quad (A5)$$

The parameters p and q are determined from r,

$$p,q = \tfrac{1}{2}\left[(r-2) \pm r(r+2) \times \left\{\frac{\beta_1}{\beta_1^2(r+2)^2 + 16(r+1)}\right\}^{1/2}\right]. \quad (A6)$$

with $p < q$ if $\beta_1 > 0$ and $p > q$ if $\beta_1 < 0$. There are additional formulas to evaluate a and b, but we need not worry about them. Full details of the complete algorithm are given in Elderton and Johnson.[22]

[1] M. Born and E. Wolf, *Principles of Optics*, 3rd ed. (Pergamon, New York, 1965).
[2] J. Perina, *Coherence of Light* (Van Nostrand Reinhold, London, 1972), p. 55.
[3] E. Wolf, "Is a complete determination of the energy spectrum of light possible from measurements of the degree of coherence?," Proc. Phys. Soc. London **80,** 1269–1272 (1962).
[4] A. Walther, "The question of phase retrieval in optics," Opt. Acta **10,** 41–49 (1963).
[5] M. L. Goldberger, H. W. Lewis, and K. M. Watson, "Use of intensity correlations to determine the phase of a scattering amplitude," Phys. Rev. **132** 2764–2787 (1963).
[6] H. Nussenzveig, "Phase problem in coherence theory," J. Math. Phys. **8,** 561–572 (1967).
[7] R. A. Gonsalves, "Phase retrieval from modulus data," J. Opt. Soc. Am. **66,** 961–964 (1976).
[8] J. R. Fienup, "Reconstruction of an object from the modulus of its Fourier transform," Opt. Lett. **3,** 27–29 (1978).
[9] R. E. Burge, M. A. Fiddy, M. Nieto-Vesperinas, and M. W. L. Wheeler, "The phase problem in scattering theory: the zeros of entire functions and their significance," Proc. R. Soc. London Ser. A **360,** 25–45 (1978).
[10] W. O. Saxton, *Computer Techniques for Image Processing in Electron Microscopy* (Academic, New York, 1978).
[11] *Inverse Source Problems in Optics*, edited by H. P. Baltes (Springer-Verlag, Berlin, 1978).
[12] E. J. Akutowicz, "On the determination of the phase of a Fourier integral, I." Trans. Am. Math. Soc. **83,** 179–192 (1956).
[13] E. J. Akutowicz, "On the determination of the phase of a Fourier integral, II." Proc. Am. Math. Soc. **8,** 234–238 (1957).
[14] P. J. Napier, "The brightness temperature distributions defined by a measured intensity interferogram," N. Z. J. Sci. **15,** 342–355 (1972).
[15] F. J. Ynduráin, "The moment problem and applications," in *Padé Approximants*, edited by P. Graves-Morris (Institute of Physics, London, 1973), p. 45.
[16] J. A. Shotat and J. D. Tamarkin, *The Problem of Moments* (American Mathematical Society, Providence, 1950).
[17] R. P. Boas, *Entire Functions* (Academic, New York, 1954), p. 103.
[18] E. C. Titchmarsh, "The zeros of certain integral functions," Proc. London Math. Soc. **25,** 283–302 (1926).

[19]B. Ya. Levin, *Distribution of Zeros of Entire Functions* (American Mathematical Society, Providence, 1964).
[20]P. Henrici, *Applied and Computational Complex Analysis* (Wiley-Interscience, New York, 1974), Vols. 1 and 2.
[21]R. Fortet, *Elements of Probability Theory* (Gordon and Breach, New York, 1977), p. 271.
[22]W. Elderton and N. Johnson, *Systems of Frequency Curves* (Cambridge University, Cambridge, 1969), Chap. 4.
[23]G. N. Watson, *A Treatise on the Theory of Bessel Functions*, 2nd ed. (Cambridge University, Cambridge, 1944).
[24]*Handbook of Mathematical Functions*, edited by H. Abramowitz and I. A. Stegun, Natl. Bur. Std., U.S. Appl. Math Ser. (U.S. Government Printing Office, Washington, D. C., 1964).
[25]Lord Rayleigh, "Note on the numerical calculation of the roots of fluctuating functions," Proc. London Math. Soc. **5,** 119–124 (1874).
[26]I. N. Sneddon, *Special Functions of Mathematical Physics and Chemistry* (Interscience, New York, 1961).
[27]L. M. Delves and J. N. Lyness, "A numerical method for locating the zeros of an analytic function," Math. Comp. **21,** 543–560 (1967).
[28]C. Shannon, "A mathematical theory of communication," Bell Syst. Tech. J. **27,** 379–423 (1948); **27,** 623–656 (1948).
[29]E. T. Jaynes, "Information theory and statistical mechanics," Phys. Rev. **106,** 620–630 (1957); **107,** 17–190 (1957).
[30]L. Ronkin, *Introduction to the Theory of Entire Functions of Several Variables* (American Mathematical Society, Providence, 1974), Chap. 4.

APPENDIX

THE SHANNON NUMBER OF AN INCOHERENT DIFFRACTION IMAGE

ABSTRACT

The Shannon number of the incoherent diffraction image of a finite object is defined as the product of the Strehl criterion and the object area. The general situation where the point spread function is asymmetric is discussed and the Shannon number is expressed in terms of the singular values and singular functions of the convolution kernel integral equation governing image formation. When the point spread function is symmetric, only the singular values enter into the description of the Shannon number.

The purpose of this note is to develop an expression for the Shannon number of the incoherent image of a finite object, see Eq. 11, in the general case where the point spread function is asymmetric.

Assuming that the isoplanatic condition holds, then the relation between an incoherently radiating object o(x) of finite size (a,b) and its corresponding diffraction image h(x) is given by the convolution relation [1]

$$h(x) = \int_a^b t(x-y)\, o(y)\, dy \quad , \quad |x| < \infty \quad , \tag{1}$$

where t(x) is the point spread function of the optical system. The functions h, t, and o are real and nonnegative.

The kernel of this integral equation is generally *asymmetric* (such as for systems suffering from coma). The formal procedure for solving Eq. 1 is the Schmidt [2] theory of singular functions – singular values. It basically amounts to symmetrizing the kernel t(x-y). The first step in the procedure is to form the right and left kernels

$$t_R(x,y) \equiv \int_a^b t(x-z)\, t(y-z)\, dz \tag{2}$$

$$t_L(x,y) \equiv \int_a^b t(z-x)\, t(z-y)\, dz \quad . \tag{3}$$

It can be shown [2] that these two kernels are symmetric and nonnegative definite. Even though the original kernel $t(x-y)$ is a function of the difference $(x-y)$, there is no guarantee that t_R and t_L can be written as such.

The functions that replace the eigenfunctions for the symmetric kernel are termed *singular functions*. They are $\psi_n(x)$ and $\phi_n(x)$, associated with the right and left kernels, respectively, and satisfy the homogeneous integral equations

$$\sigma_n^2 \, \psi_n(x) = \int_a^b t_R(x,x') \quad _n(x') \, dx' \tag{4}$$

$$\sigma_n^2 \, \phi_n(x) = \int_a^b t_L(x,x') \quad _n(x') \, dx' \quad , \tag{5}$$

where σ_n^2 are the eigenvalues of $\phi_n(x)$ and also of $\psi_n(x)$. The σ_n^2 are termed the *singular values*, and can be ordered: $\sigma_1 \geq \sigma_2 \geq \sigma_3 \geq \ldots \geq 0$. The σ_n^2 are *not* the eigenvalues of $t(x-y)$, and indeed the kernel $t(x-y)$ need not have eigenvalues. The singular function sets $\{\psi_n(x)\}$ and $\{\phi_n(x)\}$ are complete and orthonormal (under fairly weak mathematical restrictions which are certainly satisfied in the situation considered); thus,

$$\int_a^b \phi_n(x) \, \phi_m(x) \, dx = \int_a^b \psi_n(x) \, \psi_m(x) \, dx = 1 \quad . \tag{6}$$

When the kernel t(x-y) is symmetric, then the singular values and singular functions reduce to eigenvalues λ_n and eigenfunctions $\phi_n(x)$

$$\lambda_n = \sigma_n \quad , \quad \psi_n(x) = \phi_n(x) \quad . \tag{7}$$

The kernel t(x-y) admits the expansion

$$t(x-y) = \sum_{n=0}^{\infty} \sigma_n \phi_n(x) \; \psi_n(y) \quad . \tag{8}$$

We can utilize Eq. 8 to obtain an expression for the Shannon number of the incoherent diffraction image of a finite object. In analogy with the investigations in [3-8] with respect to *coherent* imagery, we *define* $S^{\#}$ as

$$S^{\#} \equiv t(o)(b-a) \; , \tag{9}$$

i.e., the product of the point spread function evaluated at the paraxial image point (Strehl ratio) and the object area (b-a).

$S^{\#}$ can be expressed in terms of the singular values and singular functions. Set x = y in Eq. 8 and integrate over the object

$$\int_a^b t(o)dx = \sum_{n=o}^{\infty} \sigma_n \int_a^b \phi_n(x) \; \psi_n(x) \; dx \quad . \tag{10}$$

It follows that

$$S^{\#} = \sum_{n=0}^{\infty} k_n \sigma_n \quad , \tag{11}$$

where

$$k_n \equiv \int_a^b \phi_n(x) \psi_n(x) \, dx \quad . \tag{12}$$

Note that $k_n \leq 1$, with equality holding only when $t(x-y)$ is symmetric; in which case Eq. 11 reduces to

$$S^{\#} = \sum_{n=0}^{\infty} \lambda_n \tag{13}$$

an expression previously derived by Gori [5].

We can interpret the k_n as a measure of the degree to which the point spread function is asymmetric. *The Shannon number for* an object imaged with an asymmetric point spread function is not equal to the Shannon number for the same object imaged with a symmetric point spread function. Although (b-a) is the same in both cases, $t(o)$ for a symmetric point spread function is the maximum value of $t(x)$, whereas the maximum value of an asymmetric point spread function is generally not at $x = 0$, but at some nonzero value of x. This is evidenced in the fact that $k_n < 1$. *Thus, the singular functions ϕ_n and ψ_n as well as the singular values σ_n enter into the determination of $S^{\#}$ for an asymmetric point spread function.* Only when the point spread function is symmetric do the singular functions drop out of the description of $S^{\#}$.

REFERENCE

1. E.L. O'Neill, Introduction to Statistical Optics (Addison-Wesley, Reading, MA, 1963) p. 77.

2. F. Smithies, Integral Equations (Cambridge University Press, Cambridge, 1958) Chap. 8.

3. G. Toraldo di Francia, "Some Recent Progress in Classical Optics," Revista Nuovo Cimento 1, 460-484 (1969). Contains further references to his pioneering papers in the 1950's.

4. D. Gabor, "Light and Information," in Progress in Optics, Vol. 1, edited by E. Wolf (North-Holland, Amsterdam, 1961).

5. F. Gori and G. Guattari, "Shannon Number and Degrees of Freedom of an Image," Opt. Comm. 7, 163-165 (1973).

6. G. Toraldo di Francia, "Degrees of Freedom of an Image," J. Opt. Soc. Am. 59, 799-804 (1969).

7. M. Bendinell, A. Consortini, L. Ronchi, and B.R. Frieden, "Degrees of Freedom, and Eigenfunctions for the Noisy Image," J. Opt. Soc. Am. 64, 1498-1502 (1974). See paragraph after Eq. 27.

SUMMARY

The purpose of this section is to summarize the technical accomplishments of the contract. In this it covers both the interim report and the present final report.

The main theme of the contract is the study of methods of obtaining the wavefront aberration function of an optical system from measurements of functions that are physically related to it. Thus, the main problem is one of inversion in the presence of noisy data. Irrespective of the methods actually employed, these inversion (or deconvolution) problems are numerically unstable because of lack of sufficient information from the response measurements to infer the correct solution. Our basic approach has been to augment the data with additional knowledge of the nature of the quantity being inverted in order to make the deconvolved solution (i.e., unknown aberrated wavefront) at least physically meaningful. A variety of techniques (most unknown to the optical community) have been utilized and also developed to carry out these calculations.

We considered four aspects of this problem, they are:

1. Wavefront from the measured point spread function (Sec. 1 of interim report).

2. Wavefront from influence functions (Sec. 3 of interim report).

3. Wavefront from interferometric data (Sec. 2 of interim report and Sec. 2 of final report).

4. Beginning development of theory to obtain the wavefront by numerically stable projection operators (Sec. 1 of final report).

In Item 1, the wavefront and point spread function are related by a nonlinear integral equation of the first kind. The inversion problem was cast as a nonlinear least squares estimation problem for the values of the aberrated wavefront at N points over the aperture, given that M ($M \geq N$) noisy measurements of the point spread function. Filtered singular value decomposition was employed in order to overcome the ill conditioning due to noise in the measurements. Attention was drawn to such difficulties as nonuniqueness, sensitivity of algorithm to initial guess, etc. Illustrative numerical examples were presented; on the basis of these calculations it can be said that this method offers great promise for actual application. The main drawback appears to be that it is slow and needs a large computer (for two-dimensional situations).

In Item 2, the wavefront and the influence function over linearly related with the influence function determined empirically from an independent set of measurements. The method of singular value decomposition is outlined for this problem. Actually it is even more ill conditioned than the nonlinear problem in Item 1. For the ill-conditioned influence matrix, we must accept the fact that its rank is poorly determined numerically and changes as the (experimentally determined) matrix elements vary by very small amounts. Although this method has been used in prior work by one of the main contractors, the numerical difficulties in handling this problem were unknown to them until the principal investigator discussed the sensitivity aspects last spring. If this method is to be used, more work must be done to determine error bounds because the influence function as well as the input data are subject to uncertainty in the presence of noise. In anticipation of this, the principal investigator has continued to study and to develop stable numerical algorithms for this situation (work done on his own time).

Item 3 is a somewhat different view of the same problem, in that we utilize interferometric data to determine the aberrated wavefront. One problem that was solved was the extension of the Zernike aberration theory for constant amplitude circular apertures to annular apertures having a bell shaped radial taper

(see Sec. 2 of interim report). These aberration functions are used as basis functions for the interferometric data reduction (see Sec. 2 of final report). Both L_2 and L_1 norm reductions of the data are discussed. It is pointed out that the L_2 norm is not robust with respect to outliers in the noisy fringe data that we must expect in hostile environments. The L_1 norm is known to be robust in such situations, and a linear programming algorithm is advocated.

Item 4 is an attempt to develop an algorithm that will provide a systematic approach to the ill posed problem of extrapolation of noisy data such as is required in some attempts to determine the wavefront. In this it is an improvement over previously proposed iterative algorithms of which the best known is the Gerschberg-Saxton algorithm. The method employes projection operators in conjunction with iterative Galerkin techniques. Numerical examples discussed in the text show great promise. Because the current contract has been terminated, extensions of the analysis to more complicated situations is held in abeyance.

In addition to these four major items, there are three additional topics that grew out of the mainstream of the research. They are important in their own right. Section 3 of the final report is entitled: Upper and lower bounds on radially symmetric optical transfer functions. This problem has been of

interest to the optical diffraction community for over 30 years. In contrast to the rectangular aperture case, the least upper bound and greatest lower bound ar found to differ. The pupil functions which achieve these bounds at a given spatial frequency are determined along with the associated transfer functions.

While working on Item 1, an unsucessful attempt was made to employ moment methods. However, it was found that moment methods could be used to attack the retrieval problem in coherence theory. Section 4 of the final report summarizes the analysis.

The final item which is listed as Appendix to the final report is entitled" The Shannon number of an incoherent diffraction image. During the course of this investigation, the principal investigator engaged in conversations with scientists from several universities who are interested in wavefront deconvolution for astronomical seeing purposes. It was thought that the Shannon number of a diffraction image could be a useful merit factor during deconvolution. Unfortunately, the Shannon number as worked out by these scientists only holds for symmetric diffraction images. The purpose of this appendix is to develop the Shannon number for an asymmetric diffraction image and to show that in this, the more realistic situation, the amount of information required to calculate the Shannon number is the same as that required to solve the original problem.

addresses	number of copies
Capt Doris Hamill RADC/OCSE	5
RADC/TSLD GRIFFISS AFB NY 13441	1
RADC/DAP GRIFFISS AFB NY 13441	2
ADMINISTRATOR DEF TECH INF CTR ATTN: ~~DTIC-DDA~~ CAMERON STA BG 5 ALEXANDRIA VA 22314	12
Bolt Beranek & Newman 10 Moulton St ~~Cambridge, MA 02238~~ Attn: Dr R. Barakat	2
Aerospace Corporation ~~Attn: Mr. Steve Burrin~~ Advanced Systems Technology Division 2400 E. El Segundo Blvd. Bldg 125/1054 ~~Elsegundo, CA 90245~~	1
The Aerospace Corp. ~~Attn: Dr. Silvertooth~~ P.O. Box 92957 El Segundo, CA 90009	1
~~Air Force Wright Aeronautical Laboratory~~ FIEE ATTN: Mr. Joseph Johnson Wright Patterson AFB, OH ~~45433~~	1

address	number of copies
Airsearch Manufacturing Co. of California Attn: Mr. Oscar Buchmann ~~2525 West 190th Street~~ Torrance, CA 90509	1
Analylic Decisions Incorporated ~~Attn: Mr. Richard Mollicone~~ 5336 West Rosecrans Avenue Suite 203 ~~Lawndale, CA 22209~~	1
Analytic Decisions, Incorporated ~~Attn: Mr. Gary Glaser~~ 1401 Wilson Blvd Arlington, VA 22209	1
Center for Analysis Attn: Mr. Jim Justice 13 Corporate Plaza NNewport Beach, CA 92660	1
The Charles Stark Draper Laboratory, Inc. Attn: Dr. Keto Soosaar ~~555 Technology Square~~ Cambridge, MA 02139	1
~~Charles~~ Starke Draper Labs ~~Attn: Dr. V. Mahajan~~ 555 Technology Square MS-85 ~~Cambridge, MA 02139~~	1
~~DARPA~~/STO ~~Attn: Maj E. Deitz~~ Arlington, VA 22209	1
~~DARPA~~/STO ~~Attn: Lt. Col A. Herzberg~~ 1400 Wilson Blvd Arlington, VA 22209	1

address	number of copies
DARPA/DSO Attn: Col R. Prater 1400 Wilson Blvd Arlington, VA 22209	1
DARPA/MIS 1400 Wilson Blvd Arlington, VA 22209	1
Eastman Kodak Co. Attn: Richard Price KAD- Lincoln Plant 901 Elmgrove Rd. Rochester, N.Y. 14650	1
General Research Corporation Attn: Mr. G.R. Curry P.O. Box 3587 Santa Barbara, CA 93105	1
General Research Corporation Attn: Mr. Thomas Zakrzewski 7655 Old Springhouse Road McLean, VA 22101	1
Hughes Aircraft Company Attn: Mr. Ken Beale Centinela & Teale Streets Culver City, CA 90230	1
Hughes Aircraft Company Attn: Fritz Benning MS 6/D 126 Centinela & Teal Sts Culver City, CA 90230	1
Institute of Defense Analyses Attn: Dr. Hans Wolfhard 400 Army Navy Drive Arlington, VA 22202	1

address	number of copies
Itek Corporation Attn: Mr. Edward Galat 10 Maguire Road Lexington, MA 02173	1
Kaman Sciences Corporation Attn: Dr. Walter E. Ware 1500 Garden of Gods Road P.O. Box 7463 Colorado Springs, CO 80933	1
Lockheed Missiles & Space Company Attn: Mr. Paul Williamson 3251 Hanover Street Palo Alto, CA 94304	1
Naval Electronic Systems Command PME-106-4 Attn: Mr. Charles Good National Center I Washington, D.C. 20360	1
Naval Research Laboratory E01P0 Attn: Dr. John McCallum 4555 Overlook Ave, SW Washington, D.C. 20375	1
Naval Sea Systems Command Attn: Dr. S. Siahatgar PMS-405 NC1 Room 11N08 Washington, D.C. 20742	1
NASA Ames Research Center MS244-7 Moffett Field, CA 94035	1
OPTICAL SCIENCES CO Attn: Dr. D. Fried P.O. Box 446 Placentia, CA 92670	1

address	number of copies
Perkin-Elmer Corp Attn: Mr. N. Levinstein 100 Wooster Heights Rd. Danbury, CT 06810	1
Photon Research Associates Attn: Mr. Jim Myer P.O. Box 1318 La Jolla, CA 92038	1
Riverside Research Attn: NALO Library, Mr. Bob Passut 1701 N. Fort Myer Drive Arlington, VA 22209	1
Rockwell International Attn: Russell Loftman (Space ~~Systems Group~~) 12214 Lakewood Blvd. Downey, CA 90241 (Mail Code - SL 56)	1
Science Applications, Inc. Attn: Mr. Richard Ryan 3 Preston Court Bedford, MA 01730	1
Sensor Systems Group Attn: Joseph S. Titus 181 West Street Waltham, Mass 02154	1
Space Division Attn: Maj T. Fern SD/VLVm P.O. Box 92960 Worldway Postal Center Los Angeles, CA 90009	1

address	number of copies
TRW Attn: Mr. Len Pincus Bldg. R-5 Room 2031 Redondo Bech, CA 90278	1
University of Arizona Attn: Robert Shannon % Charles Peyton Administration Bldg. Tuscon, AZ 85721	1
U.S. Army/DARCOM Attn: Mr. Bernie Chasnov AMC Bldg 5001 Eisenhower Ave Alexandria, VA 22333	1
U.S. Army Missile Command Attn: DRSMI-RAS/Mr. Fred Haak Redstone Arsenal, AL	1
RGB Associates, Inc. Attn: Dr. Richard Barakat P.O. Box 8 Wayland, MA 01778	1
ERIM Attn: Dr. Stan Rodinson P.O. Box 8618 Ann Arbor, MI 48107	1
Itek Corp. Attn: John Watson Optical Systems Division 10 Maguire Rd. Lexington, MA 02173	1

address	number of copies
Hughes Aircraft Co. Attn: Sam Williams Centenela & Teal Streets Culver City, CA 90230	1
Eikonix Corp. Attn: Dr. Robert Gonsalves 23 Crosby Rd. Bedford, MA 01730	1
TOTAL COPIES REQUIRED	65

MISSION
of
Rome Air Development Center

RADC plans and executes research, development, test and selected acquisition programs in support of Command, Control Communications and Intelligence (C^3I) activities. Technical and engineering support within areas of technical competence is provided to ESD Program Offices (POs) and other ESD elements. The principal technical mission areas are communications, electromagnetic guidance and control, surveillance of ground and aerospace objects, intelligence data collection and handling, information system technology, ionospheric propagation, solid state sciences, microwave physics and electronic reliability, maintainability and compatibility.